

Bright Blue and White Electrophosphorescent Triarylboryl-Functionalized C^N-Chelate Pt(II) Compounds: Impact of Intramolecular Hydrogen Bonds and Ancillary Ligands

Xiang Wang, Yi-Lu Chang, Jia-Sheng Lu, T. Zhang, Zheng-Hong Lu, and Suning Wang*

New blue and blue-green phosphorescent C^N chelate Pt(II) compounds that contain a dimesitylboryl-functionalized phenyl-1,2,3-triazole ligand (Bptrz) are synthesized. The influence of three different ancillary ligands, namely acetylacetonato (acac), picolinate (pic) and pyridyl-1,2,4-triazolyl (pytrz), on phosphorescence quantum efficiency and excimer emission is examined. Pt(II) compounds with a *p*-Bptrz ligand consistently emit a blue-green color with an emission wavelength = 490–500 nm while those with a *m*-Bptrz ligand emit a blue color with $\lambda_{\text{em}} = 450\text{--}460\text{ nm}$ and a quantum efficiency as high as 0.97. In addition to the blue monomer emission peak, Pt(*m*-Bptrz)(pytrz) compounds display an excimer emission peak at ~550 nm in a solid matrix whose intensity is dependent on the substituent group on pytrz and the doping concentration. As a result of the monomer and excimer emission, bright white phosphorescence is observed for several members of Pt(*m*-Bptrz)(pytrz) compounds. Intramolecular CH...N hydrogen bonds are found to play an important role in the high stability and high phosphorescent quantum efficiency of Pt(*m*-Bptrz)(pytrz) compounds. Single-dopant blue and white electrophosphorescent devices using Pt(*m*-Bptrz)(CF₃-pytrz-Me) or Pt(*m*-Bptrz)(*t*-Bu-pytrz-Me) as the emitter are successfully fabricated. White electroluminescence devices with external quantum efficiency of 15.6% and CIE (xy) of 0.31, 0.44 are achieved.

1. Introduction

One of the key challenges in the research and the development of organic light emitting diodes (OLEDs) is efficient and stable blue phosphorescent emitters.^[1–7] To date, the most well known blue phosphorescent emitters are based on Ir(III) C^N-, C^C- or

N^N- chelate chromophores.^[1–7] Many blue phosphorescent Ir(III) compounds contain however fluorine substituted aryl chelate ligands such as 4,6-difluorophenylpyridine, which are known to suffer from a poor stability in OLEDs, likely caused by C-F bond cleavage and isomerization during the device fabrication and operation.^[8,9] The use of pyridyl-triazolyl or *N*-heterocyclic carbene (NHC) chelate chromophore ligands in combination with appropriate ancillary ligands has led to the development of very promising fluorine-free deep-blue phosphorescent Ir(III) compounds for OLEDs.^[7,10] In contrast to the extensive literature on blue phosphorescent Ir(III) compounds and the abundant examples of green, orange or red phosphorescent Pt(II) compounds,^[11–13] blue phosphorescent Pt(II) compounds remain rare and relatively unexplored.^[14–19] Although Pt(II) compounds have the well known problems: highly prone to excimer formation and intermolecular quenching owing to the flat molecular structure,^[20] they do however possess several key features including a large ligand field splitting energy and a highly tunable emission energy via MLCT and LC states. For the same chelate chromophore, the Pt(II) compounds usually possess a much higher emission energy than the corresponding Ir(III) compounds, if intermolecular interactions of the Pt(II) compounds can be minimized.^[10,13,18]

We reported recently that the use of a bulky electron-accepting group, dimesitylboryl (BMes₂), in a chelate chromophore such as phenylpyridine (ppy)^[13,18] or phenyl-NHC (C^C chelate),^[19] can greatly enhance the phosphorescent quantum efficiency of the Pt(II) compounds and their performance in OLEDs. This dramatic improvement was attributed to the diminished intermolecular interactions, the greater mixing of MLCT and ³LC states, and the electron transporting ability of the triarylboron unit in the BMes₂-functionalized compounds.^[13a] For the BMes₂-phenylpyridine system (Bppy), bright phosphorescent Pt(II) compounds with emission colors ranging from blue-green to red have been achieved and used in high performance OLEDs.^[13,18] For the BMes₂-C^C chelate system (Bcc), highly efficient blue and blue-green phosphorescent Pt(II) compounds have been achieved and demonstrated for use in OLEDs.^[19] However, because of the synthetic

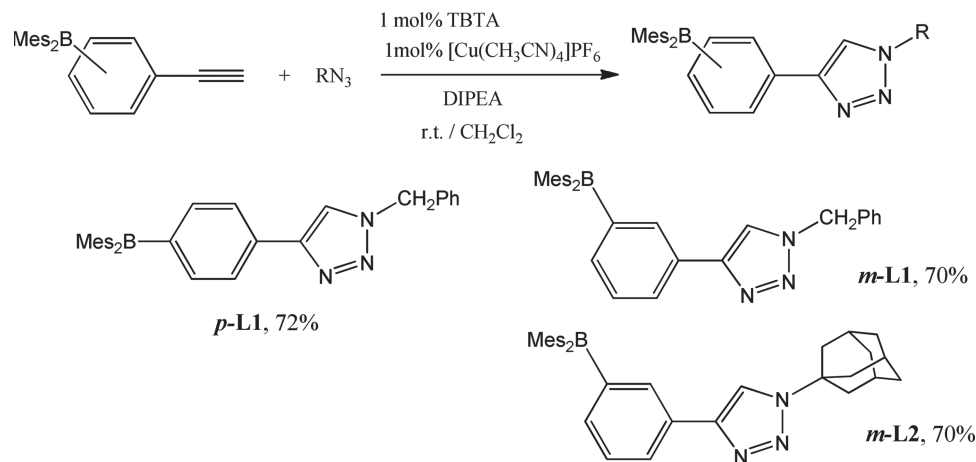
X. Wang, J.-S. Lu, Prof. S. Wang
Department of Chemistry
Queen's University
Kingston, Ontario, K7L 3N6, Canada
E-mail: wangs@chem.queensu.ca

Y.-L. Chang, Prof. Z.-H. Lu
Department of Materials Science and Engineering
University of Toronto
Toronto, Ontario, M5S 3E4, Canada

T. Zhang
School of Physical Science and Technology
Yunnan University
Kunming, Yunnan, 650091, China



DOI: 10.1002/adfm.201302871



Scheme 1. The synthetic procedure for the BMes₂-functionalized ligands.

difficulties in achieving Bcc-Pt compounds, the use of this class of compounds in OLEDs is very limited. Therefore, we initiated the investigation on new ligand systems for blue phosphorescent Pt(II) compounds. We have found that BMes₂-functionalized phenyl-1,2,3-triazole ligands (Bptrz) can lead to bright blue phosphorescent C^N chelate Pt(Bptrz)(X⁺Y⁻) compounds with the appropriate choice of the ancillary ligand X⁺Y⁻. Compared to the Bcc chelate ligands and their Pt(II) complexes, the new Bptrz chelate ligands and their Pt(II) compounds are much simpler to prepare. In addition, we have observed that the emission color and quantum efficiency of the Bptrz system are highly tunable by using ancillary ligands and the substituent groups. Further, we have found that intramolecular hydrogen bonds play a key role in this system. Efficient blue and white electrophosphorescent devices using single dopant have been fabricated. The details of our investigation are presented herein.

2. Syntheses

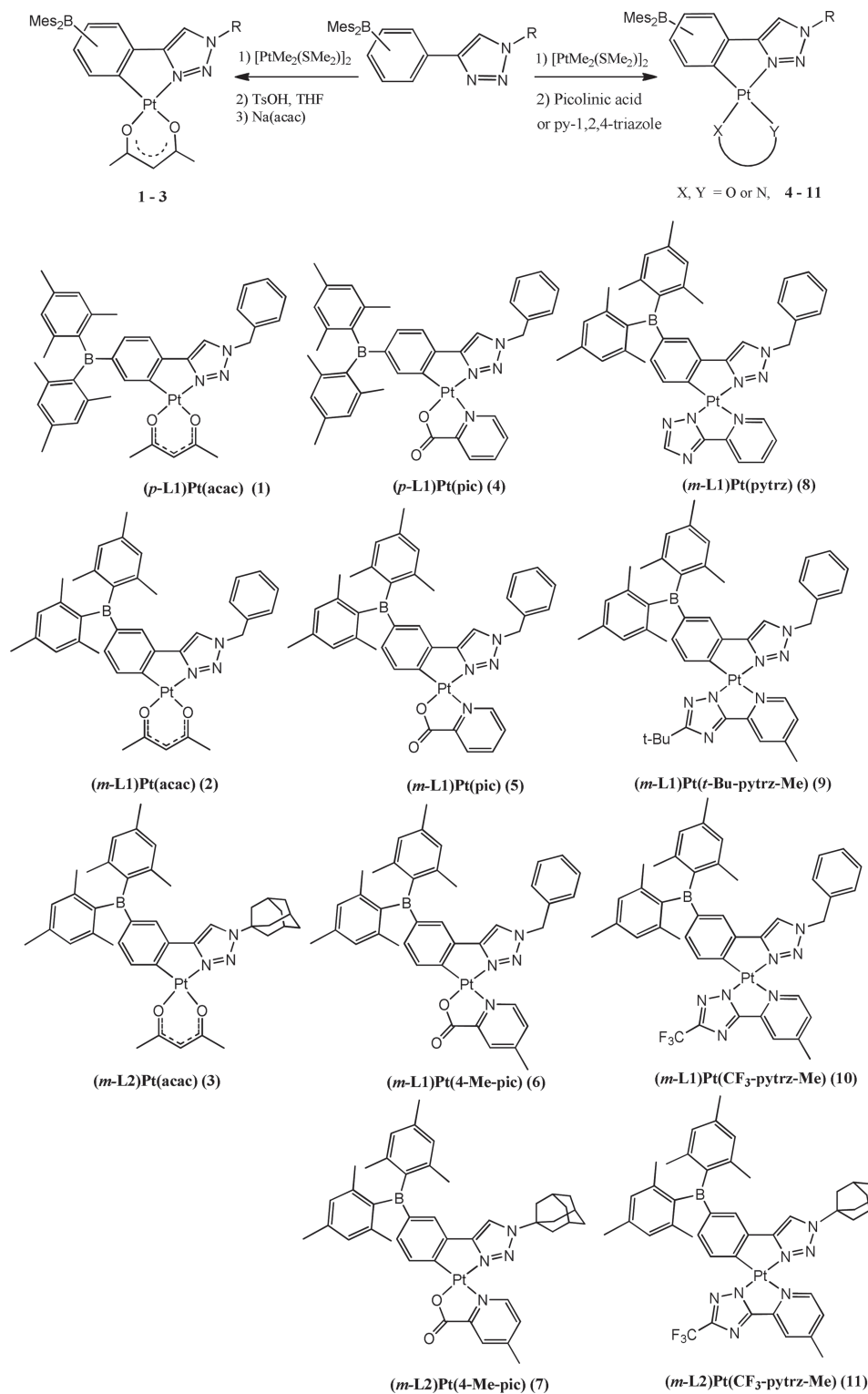
Ligand *p*-L1 is synthesized by a Cu(I) catalyzed click coupling reaction^[21–23] between (4-ethynylphenyl)dimesitylborane and benzyl azide in CH₂Cl₂ at ambient temperature. Diisopropylethylamine (DIPEA) is used as the base, and [Cu(CH₃CN)₄]PF₆ along with a stabilizing ligand tris[(1-benzyl-1*H*-1,2,3-triazol-4-yl)methyl]amine (TBTA) is used as the catalyst. Similar reactions between (3-ethynylphenyl)dimesitylborane and benzyl azide or adamantyl azide led to ligands *m*-L1 and *m*-L2, respectively (**Scheme 1**). The introduction of the adamantyl group is based on the consideration of that the free rotation of the benzyl group on the azide chromophore may cause phosphorescent quenching via intramolecular interactions with the chelate chromophore in the metal complex. Since similar intramolecular interactions are not possible for the adamantyl group, the replacement of the benzyl group by the adamantyl group could enhance the phosphorescent quantum efficiency of the Pt(II) complexes. The isolated yields of the new ligands are about 70–72%. The new BMes₂-ptrz molecules are fully characterized by nuclear magnetic resonance (NMR) and high-resolution mass spectra (HRMS) analyses.

The new Pt(II) compounds synthesized can be divided into three classes according to the ancillary ligands – acac, picolinate (pic) or substituted picolinate, and 3-(2-py)-1,2,4-triazolyl (pytrz) or substituted pytrz. For the acac and pic series, both *para* and *meta*-BMes₂ functionalized ligands *p*-L1, *m*-L1 and *m*-L2 were used. For the pytrz series, the study is focused on the *meta*-ligands, *m*-L1 and *m*-L2 only since they can produce blue phosphorescent Pt(II) compounds. The introduction of the various substituent groups is intended to minimize intermolecular interactions and tune the phosphorescent energy via induction effects.

The Pt(II) compounds are synthesized by a modified one-pot procedure (**Scheme 2**),^[24] similar to those used for Pt(Bppy)(acac) or Pt(Bppy)(pic) compounds.^[13,18,25] This procedure involves first the reaction of the Bptrz ligand with [PtMe₂(SMe₂)₂] in acetone, followed by the addition of tosylic acid (TsOH) and the subsequent addition of Na(acac) for compounds that use acac as the ancillary ligand. For compounds that use pytrz or pic as the ancillary ligands, picolinic acid or the pyridyl-1,2,4-triazole are added directly without the use of TsOH. This simple one-pot procedure leads to the isolation of the Pt(II) compounds as pure crystalline products in ~20–30% yields. All Pt(II) compounds have been fully characterized by NMR and elemental analyses.

3. Structures

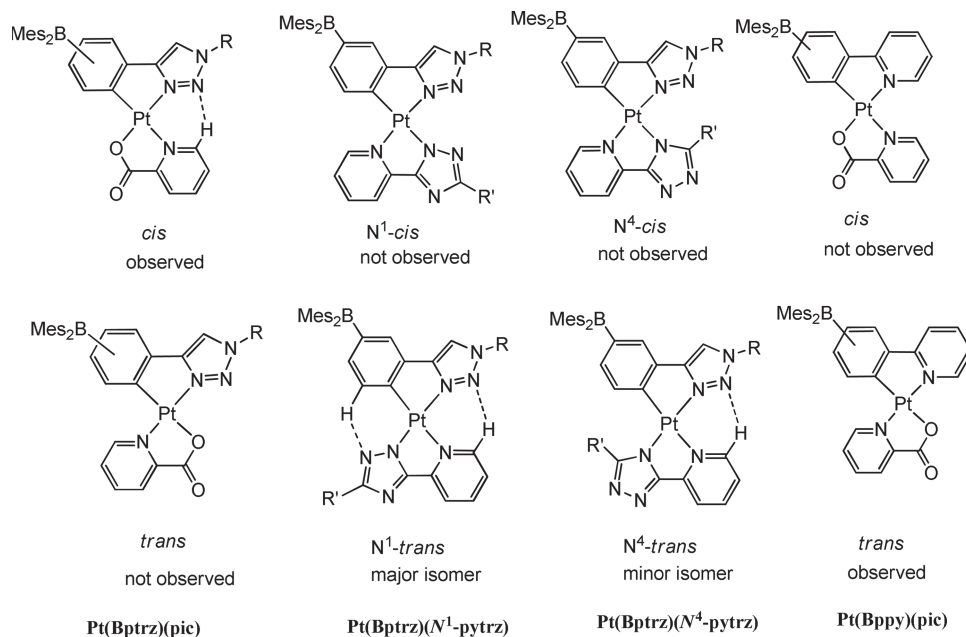
The structures of all Pt(II) compounds are established by NMR spectroscopic analyses. For Pt-pic compounds 4–7 and Pt-pytrz compounds 8–11, two geometric isomers *trans* and *cis*, as defined in **Scheme 3**, are possible. 1D and 2D NMR studies establish that the Pt-pic compounds 4–7 adopt the *cis* structure exclusively. This is in contrast to the previously reported Pt(Bppy)(pic) compounds, which adopt the *trans* structure exclusively.^[25] For the Pt-pytrz molecules, the *trans* isomer was observed exclusively. The *trans* isomers of compounds 8–11 have two possible isomers, namely the *N*¹-*trans* and *N*⁴-*trans* isomers, because of the availability of two different nitrogen binding sites of the 1,2,4-trz ring. For previously reported metal compounds with the py-1,2,4-trz ligand, both *N*¹-chelate and *N*⁴-chelate mode are



Scheme 2. The synthetic procedure and the structures of the Pt(II) compounds. THF = tetrahydrofuran.

observed.^[26] For compound **8**, the *N*⁴-*trans* isomer was found to be the major product at the early stage of the reaction while the *N*¹-*trans* isomer is the major product at the end of the reaction. Both *N*¹-*trans* and *N*⁴-*trans* isomers of **8** are isolated and fully

characterized (see supporting information) by 1D and 2D NMR spectroscopy. For compounds **9–11**, the *N*¹-*trans* isomer is the major product and fully characterized while the amount of the *N*⁴-*trans* isomer is too small for isolation.



Scheme 3. Structural Isomers of $\text{Pt}(\text{C}^{\wedge}\text{N})(\text{X}^{\wedge}\text{Y})$ compounds.

Two factors play key roles in the preferential formation of the structural isomers of the $\text{Pt}(\text{II})$ compounds shown here: *trans* influence and intramolecular H bonds. For the $\text{Pt}(\text{Bppy})(\text{pic})$ compounds, the *trans* isomer is favored by *trans* influence because the stronger pyridyl donor of the pic ligand is *cis* to the phenyl donor that has the strongest *trans* influence. In contrast, for $\text{Pt}(\text{Bptrz})(\text{pic})$ compounds 4–7, the *cis* isomer is favored because of the formation of an intramolecular H bond between the triazolyl and the pyridyl that provides a greater stability to the *cis* isomer, compared to the *trans* one. In the ^1H NMR spectra of compounds 4–7, the H^1 atom of the pyridyl ring of pic has a chemical shift at about 9.5 ppm, significantly down-fielded, compared to that of $\text{Pt}(\text{Bppy})(\text{pic})$ compounds, consistent with the *cis* structure. For the $\text{Pt}(m\text{-Bptrz})(\text{pytrz})$ compounds 8–11, the *trans* influence would favor the *cis* structure in which the two weak triazolyl donors are *cis* to each other. However, hydrogen bonding would favor the *trans*-structure since in the *trans*-structure, one or two intramolecular H bonds can form, as shown in Scheme 3, which could provide a greater

stability to the molecule than the *cis*-structure. The N^4 -*trans* isomer of 8–11 is clearly less favored than the N^1 -*trans* isomers because it has one less intramolecular H bond with unfavorable steric interactions between the R' group ($\text{R}' = \text{H}$, *t*-Bu, CF_3) of the 1,2,4-trz ring and *o*-H atom of the phenyl ring, compared to the N^1 -*trans* isomer. The formation of two intramolecular H bonds in the N^1 -*trans* isomer of 8–11 is supported by the observation of the much down-field shifted signal of the H^1 atom of the phenyl ring (~ 9.1 ppm) and that of the py ring of the pytrz ligand (~ 9.5 – 9.8 ppm) in the ^1H NMR spectra.

To further establish the structural features and the impact of different chromophores, different ancillary ligands and different substituent groups on intermolecular interactions of the $\text{Pt}(\text{II})$ compounds in the solid state, the crystal structures of 1, 4, 5, 6, 7a, 8, 9, and 10 are examined by single-crystal X-ray diffraction analyses. 7a is an analogue of 7 but without the methyl group on the py ring of pic. All structures except 5 and 8, which can be found in the Supporting Information, are shown in Figure 1, Figure 2, Figure 3, and Figure 4. Pt-ligand

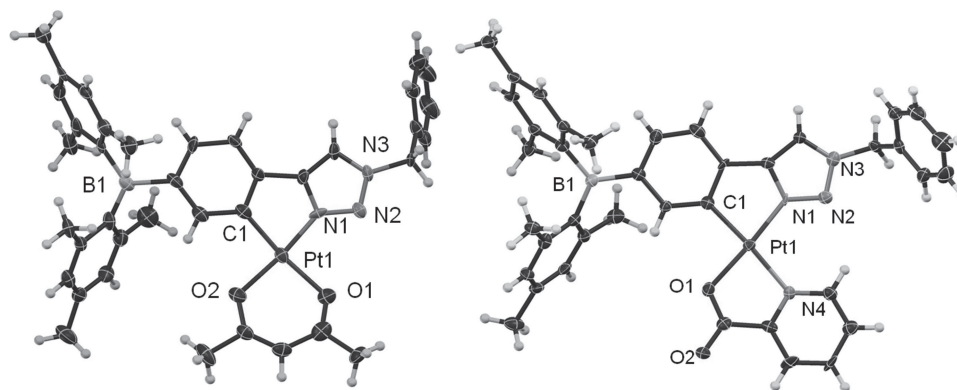


Figure 1. Crystal structures of 1 (left) and 4 (right) with 35% thermal ellipsoids and labeling schemes for key atoms.

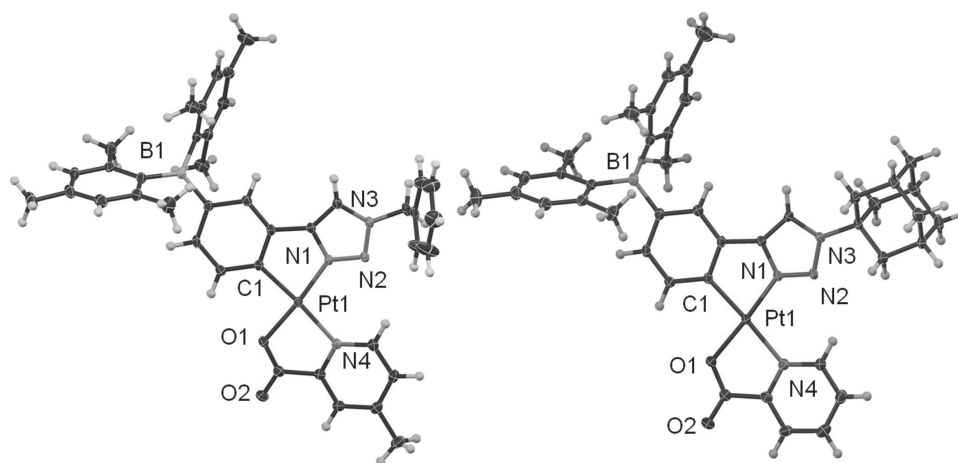


Figure 2. Crystal structures of **6** (left) and **7a** (right) with 35% thermal ellipsoids and labeling schemes for key atoms.

bond lengths are summarized in **Table 1** along with the Pt...Pt separation distances and the shortest intermolecular π stacking distances involving the central core of the Pt compounds.

The crystal structures establish several key points. The first point relates to structural isomers. As shown in Figure 2,3, the Pt(Bptrz)(pic) compounds indeed have the *cis* structure while the Pt(Bptrz)(pytrz) compounds have the *N*¹-*trans* structures. The crystal structures demonstrate that the *cis*-structure of Pt(Bptrz)(pic) compounds and the *N*¹-*trans*-structure of the Pt(Bptrz)(pytrz) compounds are indeed favored by the formation of intramolecular H bonds. The intramolecular N(2)...CH_{py} distances (Figure 2) in Pt(Bptrz)(pic) compounds **4–7a** range from 3.26 to 3.37 Å, adequate for the formation of an H bond between the trz nitrogen atom and the proton of the py ring. The intramolecular N(2)...CH_{py} distances (Figure 3 and 4) in the Pt(Bptrz)(pytrz) compounds **8–10** are 3.21 to 3.28 Å, similar to those of Pt(Bptrz)(pic). However, the N(6)...CH_{ph} distances in the Pt(Bptrz)(pytrz) compounds are shorter (3.14 to 3.18 Å), which may be attributed to the longer Pt(1)-N(4) bond, (2.129–2.147 Å), compared to the Pt(1)-N(5) bond (1.986–1.996 Å), due to the strong trans influence of the carbon donor.

The second point is regarding intermolecular interactions. The location of the BMes₂ group, the ancillary ligands, and the substituent groups do have a significant impact on intermolecular interactions. For example, (*p*-L1)Pt(acac), **1** and (*p*-L1)Pt(pic), **4** that have a similar molecular shape but with two different ancillary ligands display distinctively different intermolecular interactions (see the Supporting Information). The Pt...Pt separation distances are much greater in **1** (6.320, 6.517 Å) than **4** (4.143, 4.402 Å). In addition, molecules of **4** form partially stacked dimers with π -stacking interactions between the pic ligand and the *p*-Bptrz chelate while **1** does not have π -stacking interactions in the crystal lattice. This supports that the acac ligand is much less prone to intermolecular interactions, compared to the pic ligand. Based on the crystal structural data, compounds with either a pic or pytrz ancillary ligand have a high tendency to form π -stacked dimers or 1D extended π -stacking structures in the crystal lattice, as illustrated by the stacking diagrams of (*m*-L2)Pt(pic), (*m*-L1)Pt(pytrz), and (*m*-L1)Pt(CF₃-pytrz-Me) in Figure 4 (for other examples, please see the supporting information). This observation is not surprising since both pic and pytrz are flat chelate ligands with aryl rings.

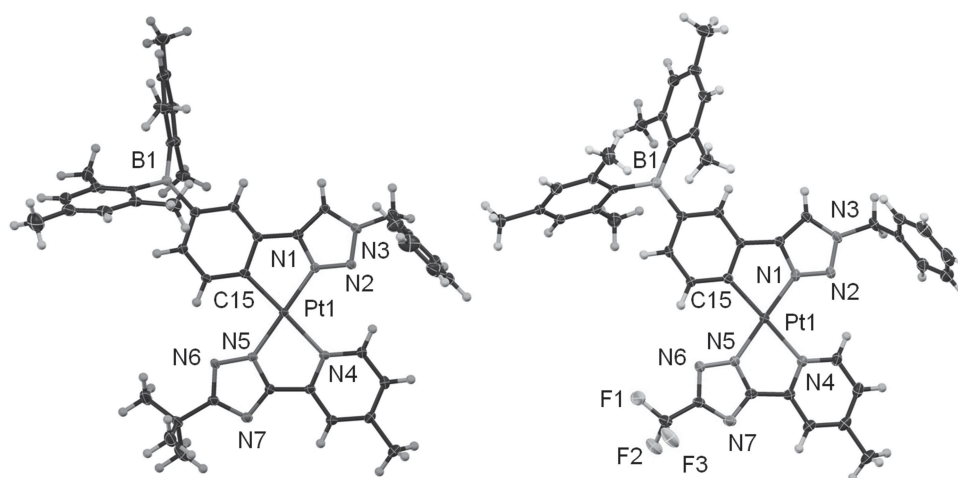


Figure 3. Crystal structures of **9** (left) and **10** (right) with 35% thermal ellipsoids and labeling schemes for key atoms.

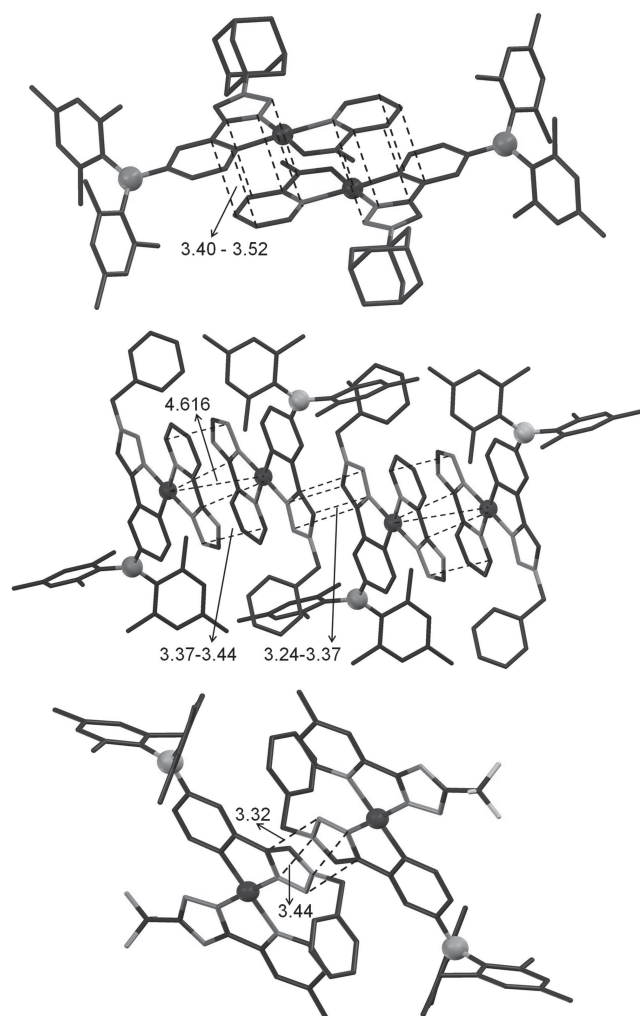
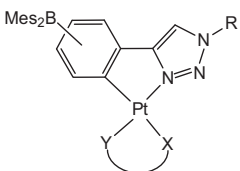


Figure 4. Top: A diagram showing the π -stacked dimer of $(m-L2)Pt(pic)$ (**7a**) in the crystal lattice. Middle: A diagram showing the 1D extended π -stacking interactions of $(m-L1)Pt(pytrz)$ (**8**) in the crystal lattice. Bottom: A diagram showing the π -stacked dimer of $(m-L1)Pt(CF_3\text{-pytrz-Me})$ (**10**) in the crystal lattice.

Table 1. Key bond lengths and short contact distances [Å].

	Pt-C	Pt-N (C [^] N)	Pt-X	Pt-Y	Pt...Pt	Shortest π stacking distance of the central core
$(p-L1)Pt(acac)$ (1)	1.980(2)	1.998(12)	2.057(13)	1.998(12)	6.517(1)	3.20(1), 3.51(1)
$(p-L1)Pt(pic)$ (4)	1.980(2)	2.000(2)	2.028(14)	1.935(12)	6.320(1)	
	2.003(10)	1.979(8)	2.107(8)	2.034(7)	4.143(1)	3.44(1), 3.46(1)
	2.004(10)	2.003(8)	2.113(8)	2.019(7)	4.402(1)	3.48(1), 3.52(1)
$(m-L1)Pt(pic)$ (5)	2.000(3)	1.972(3)	2.099(3)	2.023(2)	4.286(1)	3.40(1), 3.52(1)
$(m-L1)Pt(4\text{-Me-pic})$ (6)	1.988(3)	1.980(2)	2.102(2)	2.009(2)	4.912(1)	3.34(1), 3.40(1)
$(m-L2)Pt(pic)$ (7a)	1.998(3)	1.976(3)	2.097(3)	2.012(2)	4.209(1)	3.46(1), 3.48(1)
$(m-L1)Pt(pytrz)$ (8)	2.002(7)	2.002(6)	2.129(6)	1.987(6)	4.616(1)	3.24(1), 3.37(1) (1D stacking)
$(m-L1)Pt(t\text{-Bu-pytrz-Me})$ (9)	2.003(4)	2.004(3)	2.147(3)	1.996(3)	5.810(1)	3.34(1), 3.53(1)
$(m-L1)Pt(CF_3\text{-pytrz-Me})$ (10)	2.007(5)	1.999(4)	2.134(4)	1.995(4)	6.029(1)	3.32(1), 3.44(1)

Compound **8** is the only molecule that displays extended 1D-parallel π stacking among all the molecules examined in this work. The introduction of a substituent group on the ancillary ligand has been found to greatly diminish the extent of π stacking. For example, a methyl on the py ring and a CF_3 or a *t*-butyl group on the trz ring of the pytrz ligand reduces the 1D π -stacking in the lattice of $(m-L1)Pt(pytrz)$ to dimer π -stacking only in $(m-L1)Pt(CF_3\text{-pytrz-Me})$ and $(m-L1)Pt(CF_3\text{-pytrz-Me})$, accompanied by the substantial increase of the Pt...Pt separation distances. Another interesting aspect is that the π -stacking in the $Pt(Btrz)(pytrz)$ compounds always occurs between the same ligand, i.e., pytrz-pytrz stacking or Bptrz-Bptrz stacking (Figure 4 and the Supporting Information), involving mostly the trz ring. The replacement of the benzyl group on the Bptrz ligand by an adamantyl group does not appear to alter the π -stacking pattern, as evidenced by the similar π -stacked dimers and the similar Pt...Pt separation distances in the crystal lattices of $(m-L1)Pt(pic)$ and $(m-L2)Pt(pic)$ (see the Supporting Information).

Pt(II) complexes have a great tendency to aggregate, forming extended 1D structures in the solid state, via either Pt...Pt interactions (with very short Pt...Pt separation distances) or π ... π stacking.^[27–29] The crystal structural data of the new Bptrz-Pt(II) compounds confirmed that the bulky BMes₂ group can greatly reduce the aggregation formation of the Pt(II) compounds with intermolecular interactions limited mostly to partially π -stacked dimers. This is consistent with the general trend observed previously in Bppy-Pt(II) compounds.^[13,18]

4. Photoluminescence

4.1. Free Ligands

The free ligands *p*-L1, *m*-L1 and *m*-L2 are all purple-blue fluorescent with the emission wavelength maximum, λ_{max} , at ~400 nm in CH_2Cl_2 with a strong absorption band at ~327 nm. However, interestingly, the extinction coefficient of *p*-L1 of this band ($\epsilon = 3.32 \times 10^4 \text{ M}^{-1} \text{ cm}^{-1}$) is about 4 times that of *m*-L1

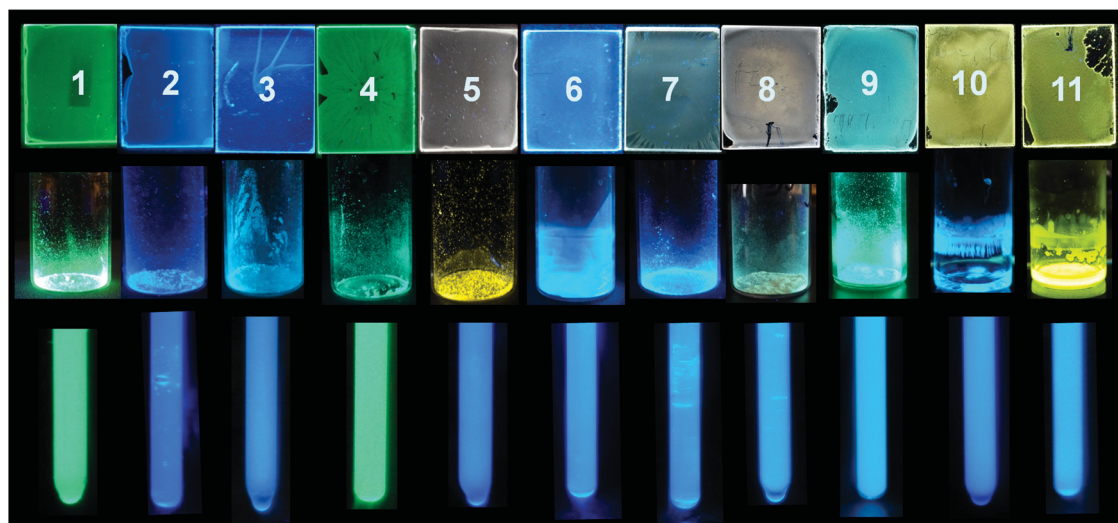


Figure 5. Photographs showing the emission colors of compounds 1–11 in 10 wt% PMMA films (top), as neat solids (middle) and in Me-THF solution ($\sim 1.0 \times 10^{-5}$ M, bottom)

and *m*-L2. TD-DFT computational studies (see Supporting Information) establish that the HOMO-1 to LUMO transition (mesityl to B-phenyl charge transfer) dominates the $S_0 \rightarrow S_1$ transition while HOMO to LUMO transition (a mixture of mesityl to B-phenyl CT and π to π^* of the ptrz backbone for *p*-L1, π to π^* of ptrz for *m*-L1) dominates the $S_0 \rightarrow S_2$ transition for *p*-L1 and *m*-L1. The $S_0 \rightarrow S_1$ transition has a similar oscillator strength for both compounds. However, the $S_0 \rightarrow S_2$ transition of *p*-L1 has an oscillator strength of 0.2534, much greater than that of *m*-L1 (0.0531), which can be attributed to the greater CT character, compared to that of *m*-L1, and is clearly responsible for the intense absorption band of *p*-L1.

4.2. Pt(II) Compounds

The Pt(II) compounds 1–11 display phosphorescence in the blue-green region (Figure 5) and the details are summarized in Table 2. In the absorption spectra, the ligand centered transition bands and the metal-to-ligand charge transfer (MLCT) transition bands overlap and are not well resolved except compound 1 that displays a distinct low energy MLCT band. Compounds 1–11 display weak phosphorescence in solution at ambient temperature with a photoluminescence quantum yield (Φ_{PL}) of $\sim 0.1\%$ to 16%. They, however display bright phosphorescence in solution at low temperature, as neat solids or in poly(methyl methacrylate)

Table 2. Photophysical data of Pt(II) Compounds.

Compound ^{a)}	Absorption ^{b)} λ_{max} [nm] ϵ [10 ⁴ cm ⁻¹ M ⁻¹]	Emission, λ_{max} [nm], 298 K						Emission 77 K ^{d)}	
		λ_{max} [nm]			Φ_{PL} ^{c)}			λ_{max} [nm]	τ_{p} [μ s]
		Me-THF	PMMA (wt%)		Me-THF	PMMA (wt%)			
			5%	10%		5%	10%		
(<i>p</i> -L1)Pt(acac) (1)	321 (2.85), 388 (0.55)	500	493	493	0.17		0.63	491	36.1
(<i>m</i> -L1)Pt(acac) (2)	326 (2.45), 362 (2.58)	453	471	471	<0.001		0.10	450	27.8
(<i>m</i> -L2)Pt(acac) (3)	325 (1.79), 345 (1.73), 358 (1.69)	451	455	455	<0.001		0.09	450	30.2
(<i>p</i> -L1)Pt(pic) (4)	292 (2.00), 328 (2.70)	489		487	0.05		0.54	483	28.2
(<i>m</i> -L1)Pt(pic) (5)	274 (1.99), 306 (1.68), 358 (2.01)	456		455, 567	<0.001		0.18	454	16.8
(<i>m</i> -L1)Pt(4-Me-pic) (6)	274 (2.21), 309 (1.72), 332 (2.03), 337 (1.97)	457	454	456	<0.001	0.34	0.24	452	16.3
(<i>m</i> -L2)Pt(4-Me-pic) (7)	272 (2.18), 334 (1.96), 352 (2.03)	456	454	454, 559	0.005	0.21	0.14	453	15.7
(<i>m</i> -L1)Pt(pytrz) (8)	320 (1.95), 362 (3.00)	464	460	460	0.01	0.82	0.59	455	11.3
(<i>m</i> -L1)Pt(<i>t</i> -Bu-pytrz-Me) (9)	321 (2.24), 364 (3.97)	474	464	466	0.10	0.97	0.65	457	9.6
(<i>m</i> -L1) Pt(CF ₃ -pytrz-Me) (10)	312 (1.96), 355 (2.97)	460	456, 554	562	0.005	0.71	0.47	454	14.3
(<i>m</i> -L2)Pt(CF ₃ -pytrz-Me) (11)	270 (2.81), 340 (1.96), 355 (2.96)	460	548	556	0.005	0.27	0.20	457	14.6

^{a)}For compounds 8–11, the data are for the *N*¹-*trans* isomers; ^{b)}Measured in Me-THF at 2×10^{-5} M; ^{c)}The solution quantum efficiency was determined in Me-THF using 9,10-diphenylanthracene as the reference under nitrogen. The solid state quantum efficiency was measured using an integration sphere. All quantum yields are $\pm 10\%$; ^{d)}Recorded in Me-THF ($\sim 1.0 \times 10^{-5}$ M).

(PMMA) films at ambient temperature. The emission spectra of compounds 1–11 in PMMA (5 wt% or 10 wt%) and in a frozen solution (see Supporting Information) all have well resolved vibronic features, an indication that the emission is mostly likely from a ^3LC state with MLCT contributions. The location of the BMes_2 group, the ancillary ligands, and the substituent groups have a significant impact on the emission color and quantum efficiency of this class of compounds.

4.3. Bptrz Ligands and the Location of the BMes_2 Group

As shown in Figure 5 and Table 2, the majority of compounds 1–11 emit a blue color ($\lambda_{\text{em}} = 450\text{--}460\text{ nm}$) in solution (at concentrations $\leq 1.0 \times 10^{-5}\text{ M}$) with the exception of compounds 1 and 4 that display a blue-green color ($\lambda_{\text{em}} = 490\text{--}500\text{ nm}$). The chelate chromophore for 1 and 4 is *p*-L1 (*p*-Bptrz-bz) while the chelate chromophore for all other compounds are either *m*-L1 (*m*-Bptrz-bz) or *m*-L2 (*m*-Bptrz-adamantyl). Thus, the BMes_2 group at the *meta* position of the phenyl ring significantly blue shifts the emission energy, compared to that at the *para* position. This observation is consistent with our earlier observation for $\text{Pt}(\text{p-Bppy})(\text{acac})$ ($\lambda_{\text{em}} = 538\text{ nm}$)^[13] and $\text{Pt}(\text{m-Bppy})(\text{acac})$ ($\lambda_{\text{em}} = 481\text{ nm}$)^[18] and attributable to the effective stabilization of the HOMO level by the BMes_2 group at the *meta*-position of the phenyl ring that widens the optical energy gap. Compared to the corresponding $\text{Pt}(\text{Bppy})(\text{acac})$ and $\text{Pt}(\text{Bppy})(\text{pic})$ ^[25] compounds, however, the emission energy of Bptrz-Pt compounds is about 30–50 nm blue shifted (e.g., $\lambda_{\text{em}} = 490\text{ nm}$ and 538 nm for 1 and $\text{Pt}(\text{p-Bppy})(\text{acac})$, respectively; 450 nm and 490 nm for 5 and $\text{Pt}(\text{m-Bppy})(\text{pic})$, respectively). This supports that the *m*-Bptrz ligands are indeed effective in achieving blue phosphorescent Pt(II) compounds.

From the phosphorescence spectra shown in Figure 6, it is also evident that compounds with the *p*-L1 chelate ligand is much less prone to the formation of excimer emission. For example, among the Pt-pic compounds, compound 4 is the only one that does not show significant excimer emission at 10 wt% doping level in PMMA, indicating that the bulky BMes_2 group is more effective in preventing intermolecular interactions at the *para* position than the *meta* position. This is not surprising since the *meta* substitution gives much greater exposure of the central core of the molecule than the *para* substitution does. Nonetheless, because the *m*-Bptrz chelate ligands lead to blue phosphorescence, this study is focused on Pt(II) compounds that contain either the *m*-L1 or *m*-L2 ligand.

Compared to the corresponding $\text{Pt}(\text{p-Bppy})(\text{acac})$ and $\text{Pt}(\text{m-ppy})(\text{acac})$ ($\Phi_{\text{PL}} = 0.77, 0.43$, respectively in CH_2Cl_2) the emission quantum efficiencies of compounds 1–3 are much lower in solution at ambient temperature (0.001–0.16 in Me-THF), which can be attributed to the much longer decay lifetimes of 1–3 (30–36 μs at 77 K), relative to those of $\text{Pt}(\text{p-Bppy})(\text{acac})$ and $\text{Pt}(\text{m-ppy})(\text{acac})$ ($\sim 10\text{ }\mu\text{s}$ at 77 K), causing efficient collisional quenching by solvent molecules in 1–3. The rotational motion of the benzyl or the adamantyl group on the trz ring may also contribute to thermal quenching of phosphorescence in these molecules. In PMMA film (10 wt%), the Φ_{PL} of 1 (0.63) is comparable to that of $\text{Pt}(\text{p-Bppy})(\text{acac})$ (0.57) while those of the blue phosphorescent 2 and 3 (0.10 and 0.09, respectively) are still lower than that of $\text{Pt}(\text{m-Bppy})(\text{acac})$ (0.35). This can be attributed to the higher triplet energy of 2

and 3 and the weaker ligand field of the Bptrz ligand, compared to the Bppy ligand in $\text{Pt}(\text{m-Bppy})(\text{acac})$, leading to a greater thermal quenching by the d-d excited state. Thus, in order to achieve bright blue phosphorescence based on the *m*-Bptrz ligand, it is necessary to replace the weak acac ancillary ligand by other ancillary ligands such as pic and pytrz to increase the ligand field strength.

4.4. Ancillary Ligands

As shown by the data in Table 2, for the same C^N ligand, replacing the acac ancillary ligand with pic or pytrz or their

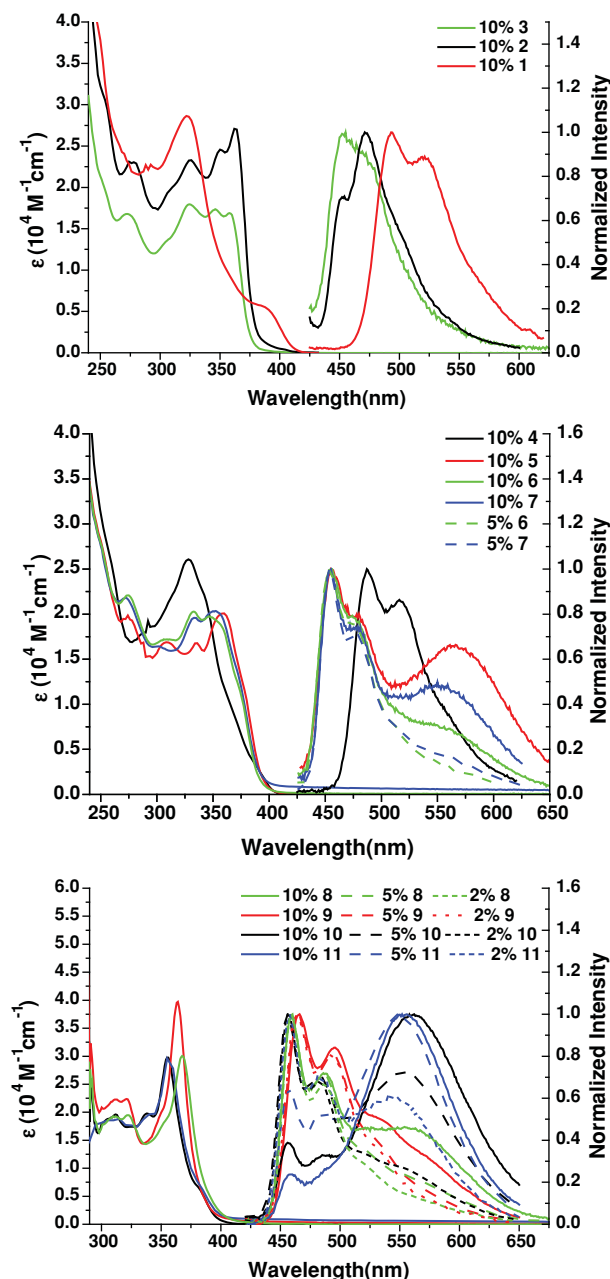


Figure 6. Absorption (left, recorded in THF) and phosphorescent spectra (right, in PMMA film with the doping level indicated) of compounds 1–11 at ambient temperature.

derivatives only leads to a small change on the phosphorescence wavelength (λ_{max} shift by ~ 5 – 15 nm). In solution at ambient temperature, the Pt-pic and Pt-pytrz compounds all have a low Φ_{PL} , which is again attributed to thermal quenching by solvent molecules and the substituent groups of the trz ring. They, however, display bright phosphorescence in PMMA films or as neat solid. At a low doping concentration (2 wt% or 5 wt%) in a polymer matrix (PMMA) or in a frozen solution, Pt(*m*-Bptrz) compounds that contain the *m*-L1 or *m*-L2 ligand all display blue phosphorescence, regardless of the ancillary ligand. The key impact of the different ancillary ligands is on the phosphorescent efficiency. Among the Pt(*m*-Bptrz) compounds, the phosphorescent quantum efficiency follows the order of $9 > 8 > 10 > 6 > 7 \approx 5 > 3 \approx 2$. Compounds with the acac ancillary ligand have the lowest blue phosphorescence efficiency (~ 0.10 at 5–10 wt% in PMMA) while compounds with the pytrz ancillary ligand have the highest and very impressive blue phosphorescence efficiency (0.71–0.97 in 5 wt% PMMA, ~ 0.50 in 10 wt% PMMA). One key improvement from the acac to the pytrz ancillary ligand is the significant shortening of the decay lifetime from ~ 30 μs to ~ 10 – 15 μs . The influence of the ancillary ligands on the blue phosphorescent Φ_{PL} of compounds 2, 3, 5–10 can be explained by the ligand field strength of the ancillary ligands that follows the order of pytrz > pic > acac. Based on the decay lifetimes and the phosphorescent quantum efficiencies, for the same C^N ligand, the k_{r} increases in the order of Pt-pytrz > Pt-pic > Pt-acac, in agreement with the order of the ligand field strength, thus illustrating that using ancillary ligands to enhance the phosphorescent efficiency is a highly effective approach. The same approach has been extensively explored in blue phosphorescent Ir(III) compounds.^[4,5,10]

The other distinct impact by different ancillary ligands is the excimer emission caused by intermolecular interactions. As shown in Figure 6, compounds 1–3 with the acac ancillary ligands display no obvious excimer emission at 10 wt% doping level in PMMA while excimer formation is evident for all other compounds except compound 4 at the same doping level. This is in agreement with the crystal structures that revealed the presence of π -stacked dimer or 1D-structures in the crystal lattices of Pt-pic and Pt-pytrz compounds which are absent in the Pt-acac compounds. The tendency of the Pt-pic compounds to form excimer emission was also observed in Pt(*m*-Bppy)(pic) previously.^[25] Because of the excimer formation, the quantum efficiency of Pt-pic and Pt-pytrz compounds decreases substantially with increasing doping concentrations in PMMA (Table 2).

4.5. Substituent Groups

For a given C^N ligand and an ancillary ligand, it is observed that the substituent group on the ancillary ligand can have a subtle

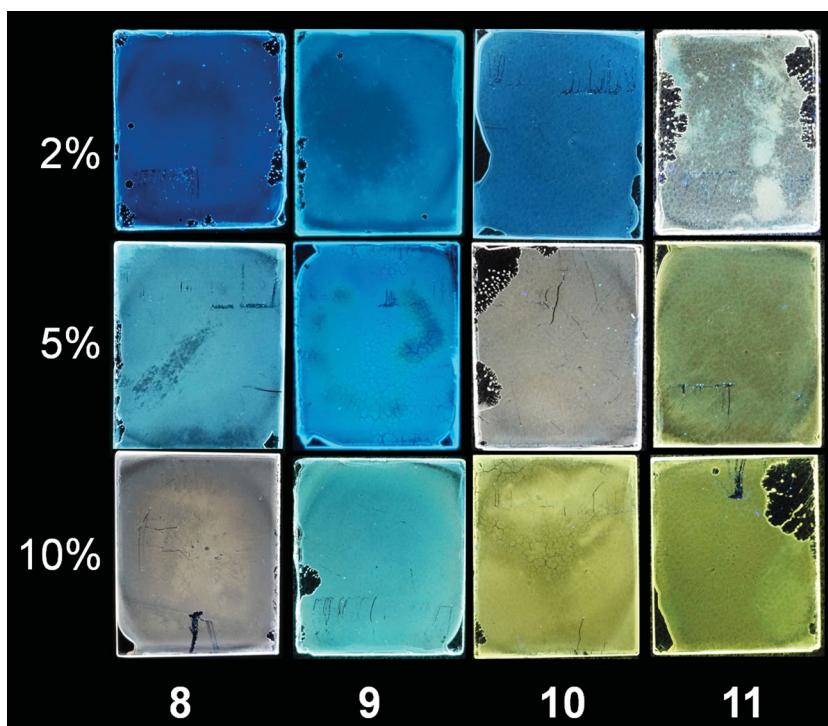


Figure 7. Photographs showing the emission colors of compounds 8–11 (*N*¹-*trans* isomers) in 2 wt%, 5 wt%, and 10 wt% PMMA films.

impact on phosphorescent energy and efficiency of the Pt(II) compounds, especially for the pic and pytrz series. The influence of substituent groups on the acac ligand is not examined since there is no strong intermolecular interactions in Pt(Bptrz)(acac) compounds and the replacement of the methyl groups by *t*-butyl groups in previously investigated Pt(C^N)(acac) and derivative compounds does not lead to any significant change of emission energy or efficiency.^[20] For the Pt-pic compounds, a methyl group at the 4-position of the py ring in the pic ligand does not change the emission color significantly but substantially decreases the excimer formation and increases the emission Φ_{PL} as shown by the data for compounds 5 and 6 in Table 2 and the spectra in Figure 6. For the Pt-pytrz compounds, the introduction of a *t*-butyl group on the trz ring and a methyl on the py ring of the pytrz ligand reduces the excimer emission and increases the emission quantum efficiency, accompanied by a few nanometer red-shift of the emission energy (see data for 8 and 9) because of the increased steric bulkiness that diminishes intermolecular interactions involving the central core. Surprisingly, the replacement of the *t*-butyl by a smaller electron-withdrawing CF₃ in compound 10 leads to a great increase of excimer emission, albeit ~ 8 nm blue shift of the monomer emission peak, compared to that of 8 and 9. Compound 10, in fact, emits a white color at 5 wt% doping level and a yellow color at 10 wt% level, as shown by the photographs in Figure 7. Despite the excimer emission, the Φ_{PL} of compound 10 remains impressive (0.71 and 0.47 for 5 wt% and 10 wt%, respectively), making it a good candidate as a single dopant for white light OLEDs.^[30,31]

To examine if the benzyl group on the trz ring of the C^N chelate ligand has any adverse effect on phosphorescent efficiency,

it is replaced by an adamantyl group in **3**, **7** and **11**. As shown by the data in Table 2, for the Pt-acac compounds, there is little difference in emission color and efficiency between the benzyl and adamantyl substituted compounds. For the Pt-pic compounds, the adamantyl group appears to increase the excimer emission and decrease the efficiency significantly as shown by the emission spectra of **6** and **7** in Figure 6 and the data in Table 2. For the Pt-pytrz compounds, the adamantyl group appears to strongly enhance excimer emission, as illustrated by compound **11**, which displays a greater tendency to produce excimer emission than the benzyl analogue **10**. The quantum efficiency of **11** also decreases significantly with the increasing doping concentration and the excimer formation ($\Phi_{\text{PL}} = 0.41$, 0.27, 0.20 at 2 wt%, 5 wt%, and 10 wt% doping level, respectively). As a consequence, the emission quantum efficiency of **11** is much lower than that of **10** at the same doping level. Based on the comparison of the Pt-pytrz compounds **10** and **11**, and Pt-pic compounds **6** and **7**, it can be concluded that the adamantyl group favors excimer emission and decreases quantum efficiency, compared to the benzyl group. This may be explained by the benzyl being more sterically demanding than adamantyl. The impact of the substituent group and the doping level on the emission color of the Pt-pytrz compounds **8–11** are illustrated by the photographs in Figure 7.

4.6. The N^1 -trans and N^4 -trans Isomers of **8**

As shown in Figure 8, both N^1 -trans and N^4 -trans isomers of **8** have the same monomer emission peak at 460 nm. However, at the 5 wt% and 10 wt% doping levels, the N^4 -trans isomer has a strong excimer emission peak at 544 nm dominates with $\Phi_{\text{phos}} = 0.54$ and 0.47, respectively. In contrast, for the N^1 -trans isomer, the 460 nm peak dominates with $\Phi_{\text{phos}} = 0.82$ and 0.59 at 5 wt% and 10 wt% doping level, respectively. This indicates that the N^4 -trans isomer of compound **8** is much more prone to excimer formation than the N^1 -trans one. The reason for this is not understood. The double intramolecular hydrogen bonds are believed to play an important role in the exceptionally bright blue phosphorescence displayed by the N^1 -trans isomers of

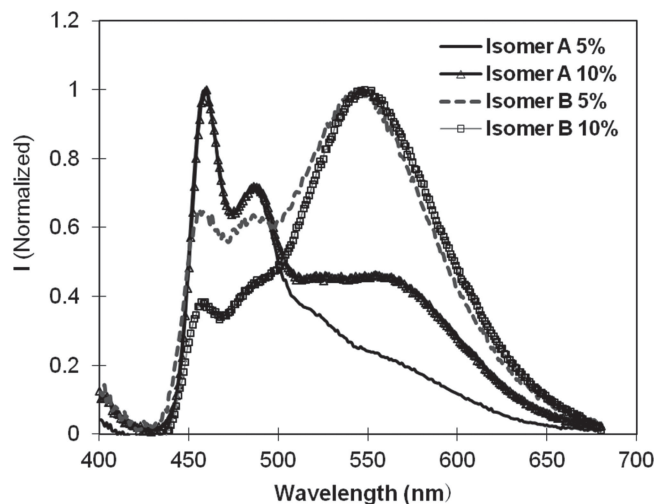


Figure 8. The phosphorescent spectra of the N^1 -trans (**A**) and N^4 -trans (**B**) isomers of compound **8** in 5 wt% and 10 wt% PMMA films.

compounds **8–11** since they greatly increase the rigidity of the molecules. Weak inter- or intramolecular $\text{CH}\cdots\text{N}$ hydrogen bonds have been demonstrated previously to greatly improve the electron transport mobility of aromatic N -heterocyclic compounds and their performance in OLEDs.^[30] The isomers of compound **8** are rare examples that illustrate the significant impact of weak intramolecular $\text{CH}\cdots\text{N}$ hydrogen bonds on phosphorescent quantum efficiency and excimer emission.

5. Computational Study

To further understand the photophysical properties of the Pt(II) compounds, TD-DFT calculations are performed for representative Pt(II) compounds using the Gaussian 03 software,^[32] at the B3LYP level of theory using LAN2LD as the basis set for Pt and 6-31G* for all other atoms and the results are summarized in Table 3. The experimentally estimated HOMO and LUMO energies using the reduction potential and the optical

Table 3. Experimental HOMO–LUMO energy and TD-DFT data for selected compounds.

	Experimental data				TD-DFT data					
	^{a)} E^{red}	HOMO ^{b)} [eV]	LUMO ^{b)} [eV]	E_{g} (T_1) ^{c)}	HOMO [eV]	LUMO [eV]	H–L gap [eV]	E_{g} (T_1) ^{d)}	% H \rightarrow L ($S_0 \rightarrow S_1$)	f ($S_0 \rightarrow S_1$)
1	–2.44	–5.38	–2.36	2.53	–5.31	–1.52	3.79	2.66	88	0.0564
2	–2.35	–5.69	–2.45	2.76	–5.42	–1.36	4.06	2.88	78	0.3752
4	–2.32	–5.53	–2.48	2.58	–5.52	–1.66	3.86	2.71	70	0.0268
5	–2.27	–5.67	–2.53	2.75	–5.63	–1.74	3.89	2.83	80	0.1249
6	–2.42	–5.53	–2.38	2.74	–5.58	–1.63	3.95	2.84	83	0.1687
7	–2.25	–5.70	–2.55	2.74	–5.52	–1.58	3.95	2.82	84	0.1632
8	–2.29	–5.61	–2.51	2.73	–5.58	–1.66	3.92	2.76	86	0.0076
9	–2.40	–5.48	–2.40	2.71	–5.39	–1.58	3.81	2.71	88	0.0008
10	–2.26	–5.66	–2.54	2.73	–5.69	–1.77	3.92	2.81	79	0.0641
11	–2.27	–5.67	–2.53	2.71	–5.63	–1.74	3.89	2.79	82	0.0654

^{a)} Recorded in $\text{CH}_3\text{CN}/\text{THF}$ with 0.10 M Bu_4NPF_6 at a scan rate of either 100 mV s^{-1} or 200 mV s^{-1} (vs. $\text{Cp}_2\text{Fe}/\text{Cp}_2\text{Fe}^+$); ^{b)} The LUMO energy was estimated using the reduction potential and the HOMO energy was calculated using the absorption edge and the LUMO energy; ^{c)} The triplet energy value (T_1) was estimated using the emission spectra at 77 K; ^{d)} $S_0 \rightarrow T_1$ vertical excitation energies.

absorption edge are also listed in Table 3 and Figure 9 for comparison. The HOMO and LUMO surfaces for selected compounds are given in Table 4. The complete data can be found in the Supporting Information.

The HOMO and LUMO levels of the Pt-acac compounds 1–2 are in general higher than those of Pt-pic (4–7) and Pt-pytrz (8–11) with 10 having the deepest HOMO and LUMO levels. For the Pt-acac compounds, the *m*-L1 ligand causes destabilization of the LUMO and stabilization of the HOMO, leading to a wider HOMO–LUMO gap and a higher triplet energy, compared to the *p*-L1 ligand (2 versus 1). For the Pt-pic compounds, the *m*-L1 ligand causes stabilization of both HOMO and LUMO levels but slightly more pronounced at the HOMO level, thus also leading to a higher triplet energy, compared to the *p*-L1 ligand (5 versus 4). Electron-donating substituent groups on the ancillary ligands destabilize both HOMO and LUMO levels while the electron withdrawing group CF₃ has the opposite effect (e.g., 5 versus 6, and 9 versus 10).

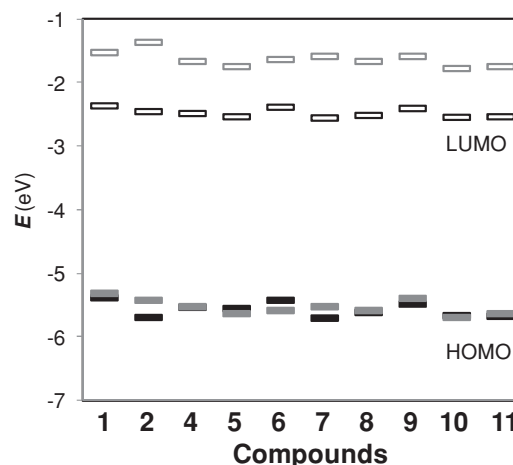


Figure 9. The experimental (black) and calculated (gray) HOMO and LUMO energies for selected compounds.

Table 4. HOMO and LUMO surfaces of Selected Pt(II) Compounds (isocontour value = 0.03).

	1	2	4	5
LUMO				
HOMO				
	6	8	9	10
LUMO				
HOMO				

TD-DFT data establish that the HOMO→LUMO transition is the main component of the $S_0 \rightarrow S_1$ and $S_0 \rightarrow T_1$ transitions for all compounds and the ancillary ligand contributes to either HOMO or LUMO or both. For the Pt-acac compounds, the HOMO has contributions mainly from the acac ligand, the Pt d orbital and the phenyl ring of the Bptrz ligand while the LUMO is localized on the Bptrz chelate with a large contribution from the boron center. For Pt-pic compounds, the HOMO involves mainly the phenyl ring and the mesityl ring of the Bptrz ligand, and the Pt d orbital while the LUMO has major contributions from the pic ligand and the B atom of the Bptrz ligand. The acac contributions to the HOMO level in Pt-acac compounds is likely responsible for the higher HOMO energy level of **1**, relative to that of **4**. The involvement of the pic ligand in the LUMO level stabilizes LUMO of **4**, relative to that of **1**. For the Pt-pytrz compound **8**, the HOMO and LUMO are delocalized over the Bptrz and the pytrz ligand with the Pt d orbital contributing to the HOMO and the B π orbital contributing to the LUMO. The LUMO of **9** and **10** resembles that of **8**. However, the HOMO of **9** has no contributions from the Bptrz ligand while the HOMO of **10** has no contributions from the pytrz ligand. This can be explained by the nature of the substituent group on the pytrz ligand. The electron donating *t*-butyl group destabilizes the π orbital of the pytrz such that it dominates the HOMO, causing the slightly narrowing of the HOMO-LUMO gap of **9**, relative to **8**. In contrast, the electron withdrawing CF_3 group stabilizes the π orbital of the pytrz such that it no longer contributes to the HOMO, causing the slightly widening of

the HOMO-LUMO gap of **10**, relative to **9**. The computational data show that the replacement of the benzyl group by an adamantyl group in the Bptrz ligand causes a slight destabilization of both HOMO and LUMO levels, but more pronounced on the HOMO, leading to a slight narrowing of the HOMO-LUMO gap (e.g., **2** versus **3**, **5** versus **7**, **10** versus **11**). Based on the computational data, the phosphorescence of compounds **1–11** are mainly from mainly from ^3LC of Bptrz mixed with MLCT and inter-ligand charge transfer transitions.

6. Electrophosphorescence

The study of electroluminescent (EL) properties is focused on them. Compounds **9** and **10** are chosen for EL evaluation, based on the following considerations. (1) **9** is the most efficient blue phosphorescent emitter and has the least tendency to form excimer emission among the Pt(Bptrz)(pytrz) compounds, thus most suitable for blue phosphorescent OLEDs. (2) **10** is a deep blue emitter but shows a great tendency to form excimer, producing white light emission with impressive quantum efficiency, thus, may be suitable as a single dopant for white light OLEDs. (3) Both **9** and **10** display a high thermal stability with the decomposition temperature being $>280^\circ\text{C}$ for **9** and $\sim 250^\circ\text{C}$ for **10**, based on DSC data.

The basic EL device structure used in the study is shown in **Figure 10**. For the electron transporting layer, both TPBi and TmPyPb are examined. EL devices using TmPyPb as the ETL

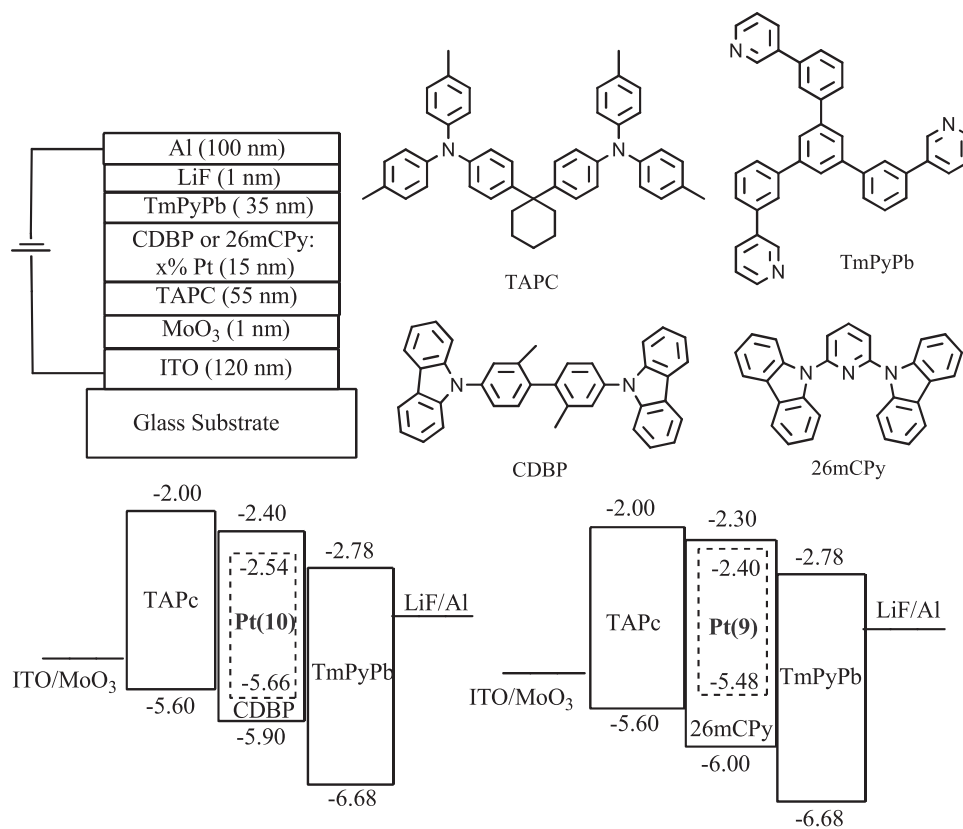


Figure 10. EL device structure and materials used.

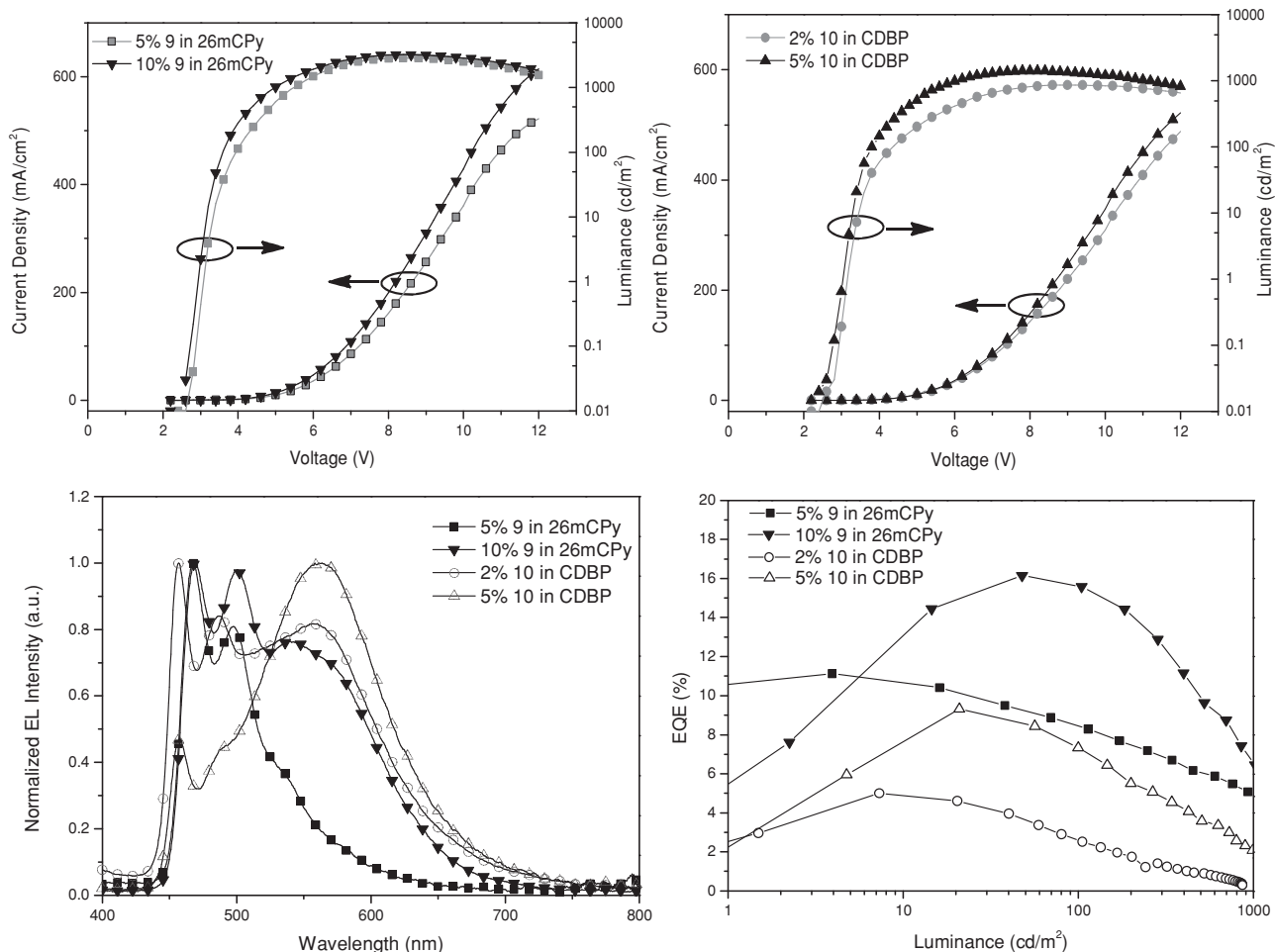


Figure 11. EL spectra, luminance–current density–voltage (L–J–V), and external quantum efficiency (EQE)–L diagrams of EL devices using **9** or **10** as the dopant.

consistently give better performance, perhaps because of the higher triplet energy of TmPyPb, compared to TPBi.^[33] For the hole transport layer, TAPc is used because its energy levels match well those of the host materials. Both CDBP and 26mCPY are chosen as the host materials because of their high triplet energies^[33] (3.0 eV and 2.9 eV, respectively). For compound **9**, 26mCPY is found to be a better host than CDBP while for **10**, CDBP is found to produce more efficient devices than 26mCPY. The distinct dependence of EL devices of **9** and **10** on the host material can be explained by the energy level diagrams shown

in Figure 13, which illustrate that 26mCPY allows better exciton confinement for **9** while CDBP for **10**. Based on the photoluminescent data, EL devices with doping level at 2%, 5%, and 10% for **9**, and at 2% and 5% for **10** were fabricated with the aim to achieve blue and white EL. The EL data for 5% and 10% devices of **9** and 2% and 5% devices of **10** are shown in Figure 11 and Table 5. The EL spectrum of the 5% device of **9** matches very well with the PL spectrum in 5 wt% PMMA or 26mCPY, producing a sky blue color with $\lambda_{\text{em}} = 467$ nm and CIE(xy) of 0.19, 0.34. At 10% doping level, although the EL spectrum of **9** is still

Table 5. EL device data for **9** and **10**.

Device	EL λ_{max} [nm] ^{a)}			η_{ext} [%] ^{d)}			CIE		
	V_{on} [V] ^{b)}	L [cd/m ² , V] ^{c)}		10 cd/m ²	100 cd/m ²	1000 cd/m ²	η_c [cd/A] ^{e)}	η_p [lm/W] ^{e)}	(x,y)
5% 9	467	3.2	2879, 8.4	10.4	8.3	4.6	23.6	23.2	(0.19, 0.34)
10% 9	468	3.0	3220, 8.6	14.4	15.6	6.5	36.7	33.9	(0.31, 0.44)
2% 10	456	3.2	865, 9.2	5.0	2.5	—	11.8	10.9	(0.32, 0.42)
5% 10	563	3.2	1420, 8.0	9.3	7.3	2.1	24.7	22.9	(0.38, 0.48)

^{a)}Value taken at $I = 20$ mA; ^{b)}The applied voltage (V_{on}) is defined as brightness of 1 cd/m²; ^{c)}The luminance (L) is the maximum value; ^{d)}External quantum efficiency (EQE, η_{ext}); ^{e)}Current efficiency (η_c) and power efficiency (η_p) are the maximum values.

dominated by the monomer peak at 467 nm, a large excimer peak at ~555 nm appears, which is again in agreement with the PL spectrum at the same doping level. As a consequence, this EL device produces a white color with CIE (xy) of 0.31, 0.44. For compound **10**, at the 2% doping level, the monomer blue peak at 456 nm dominates the EL spectrum while the contribution of the excimer peak at ~555 nm is significant, leading to a white color with CIE (xy) of 0.32, 0.42. At 5% doping level, the EL spectrum of **10** is dominated by the excimer peak, producing a yellowish white color with CIE (xy) shifting to 0.38, 0.48. The general trend of the EL spectral dependence of **10** on the doping level is in agreement with that of PL in PMMA films. However, it appears that **10** is more prone to excimer formation in the EL device than in PMMA since it has a greater excimer contribution at the same doping level in the device than in PMMA. In addition, the external quantum efficiency of EL devices of **9** and **10** increases significantly with the doping level, which contradicts the trend observed for PL that decreases in efficiency with increasing doping concentration. This could be caused by more efficient exciton confinement to the excimer than the monomer emission in the device. The other possible explanation is the reduced host triplet-triplet annihilation (TTA) with increasing doping concentration, leading to higher device efficiency.^[34] All devices have a low turn-on voltage of 3.0–3.2 V. The white 10% EL device of **9** has the most impressive performance with a maximum brightness of 3220 cd/m² and an external quantum efficiency of 15.6 at 100 cd/m². Although many examples of efficient white electrophosphorescent devices are known previously,^[31] the majority of them use either multiple dopants or tandem device structures. Efficient white electrophosphorescent devices based on single dopant remain relatively rare with several examples based on Pt(II) excimers being reported recently.^[31d,35] The performance of the 10% EL device of **9** is certainly among the most efficient single-dopant white EL devices.

7. Conclusions

A series of new blue and blue-green phosphorescent Bptrz C[∧]N chelate Pt(II) compounds are achieved. Three different classes of ancillary ligands are examined and are found to have a distinct impact on the phosphorescent quantum efficiency with the pyridyl-1,2,4-triazole (pytrz) ligand being the most effective in enhancing the blue phosphorescent quantum efficiency of the Pt(II) compounds. The double intramolecular hydrogen bonds formed between pytrz and Bptrz in the complex is found to enhance the stability and the emission efficiency of the Pt(II) compounds. Substituent groups on the ancillary ligands are found to greatly influence the extent of excimer formation and the quantum efficiency. Bright white phosphorescence as a result of the excimer and the monomer emission is observed in some of the Pt(Bptrz)(pytrz) compounds. Preliminary evaluation on the performance of two members of Pt(Bptrz)(pytrz) compounds demonstrates that they are very promising candidates in producing highly efficient blue or white phosphorescent OLEDs using single dopant. Future work will focus on the optimization and the stability of the EL devices based on the new blue and white phosphorescent Pt(II) compounds.

8. Experimental Section

8.1. General Experimental Information

All reactions were carried out under a nitrogen atmosphere unless otherwise noted. Reagents were purchased from Aldrich chemical company and used as received. TLC and flash chromatography were performed on silica gel. ¹H and ¹³C NMR spectra were recorded on Bruker Avance 300, 400, or 500 MHz spectrometers. Deuterated solvents were purchased from Cambridge Isotopes and used without drying. Excitation and emission spectra were obtained on a Photon Technologies International QuantaMaster Model 2 spectrometer. Phosphorescent decay life times were measured using a Photon Technologies International Phosphorescent lifetime spectrometer. Solid state quantum efficiency measurements were performed using an integration sphere. Phosphorescence quantum yields of compound **1**, **4**, and **8-11** were measured relative to 9,10-diphenylanthracene in degassed 2-methyltetrahydrofuran ($\Phi = 0.90$) at 298 K. UV-visible spectra were recorded using a Varian Carry 50 UV/Vis spectrophotometer. Cyclic voltammetry experiments were conducted on a BAS CV-50W analyzer with a scan rate of either 150 or 200 mVs⁻¹. The electrochemical cell was a standard three-compartment cell composed a Pt working electrode, a Pt auxiliary electrode and an Ag/AgCl reference electrode. All measurements were using 0.1 M NBu₄PF₆ in DMF as the supporting electrolyte. Ferrocene/ferrocenium was used as internal standard ($E^\circ = 0.55$ V). Elemental analyses were performed by University of Montreal Elemental Analysis Laboratory. Crystal structures were obtained using a Bruker AXS Apex II X-ray diffractometer. TD-DFT calculations were carried out using the Gaussian 03 software^[32] at the High Performance Computing Virtual Laboratory (HPCVL) at Queen's University. All computations were performed at the B3LYP level of theory using LAN2LD as the basis set for Pt and 6-31G(d) for all other atoms. *p*-(dimesitylboryl)phenylacetylene^[36] and *o*-(dimesitylboryl)phenylacetylene^[37] were prepared according to literature procedures.

8.2. Synthesis of Bptrz Ligands

4-(4-Dimesitylborylphenyl)-1-benzyl-1H-1,2,3-triazole (*p*-L1): To a 50 mL Schlenk flask with a stir bar was added *p*-(dimesitylboryl)phenylacetylene (0.64 g, 1.84 mmol), benzyl azide (0.245 g, 1.84 mmol), diisopropylethylamine (0.475 g, 3.68 mmol), tris[(1-benzyl-1H-1,2,3-triazol-4-yl)methyl]amine (1 mol %) and 30 mL of dichloromethane. The solution was degassed for 20 min before [Cu(CH₃CN)₄]PF₆ (1 mol %) was added. The resulting mixture was stirred overnight. After the solvent was removed under reduced pressure, the product was extracted with dichloromethane, and then washed with saturated ammonium chloride solution, brine and water. The combined organic phase was dried over MgSO₄, filtered and purified using flash column chromatography on silica (4:1 hexanes: ethyl acetate as eluent) to afford 0.64 g of *p*-L1 as white solid (72% yield). ¹H NMR (400 MHz, CDCl₃, δ , ppm): 7.82 (d, ³J = 8.0 Hz, 2H), 7.76 (s, 1H), 7.59 (d, ³J = 8.0 Hz, 2H), 7.42–7.32 (m, 5H), 6.86 (s, 4H), 5.61 (s, 2H), 2.34 (s, 6H), 2.05 (s, 12H). ¹³C NMR (100 MHz, CDCl₃, δ , ppm): 148.1, 145.8, 141.7, 140.9, 138.7, 137.0, 134.7, 133.7, 129.2, 128.8, 128.2, 128.0, 125.2, 120.2, 54.3, 23.5, 21.3.

4-(3-Dimesitylborylphenyl)-1-benzyl-1H-1,2,3-triazole (*m*-L1): Prepared using the same procedure as that for *p*-L1, replacing *p*-(dimesitylboryl)phenylacetylene with *o*-(dimesitylboryl)phenylacetylene (75% yield). ¹H NMR (400 MHz, CDCl₃, δ , ppm): 8.02 (d, ³J = 7.2 Hz, 2H), 7.86 (s, 1H), 7.64 (s, 1H), 7.50–7.30 (m, 7H), 6.82 (s, 4H), 5.57 (s, 2H), 2.32 (s, 6H), 2.00 (s, 12H). ¹³C NMR (100 MHz, CDCl₃, δ , ppm): 148.3, 140.9, 136.8, 136.1, 134.8, 132.9, 130.3, 129.3, 129.2, 128.8, 128.6, 128.3, 128.0, 119.8, 54.2, 23.5, 21.3.

4-(3-Dimesitylborylphenyl)-1-adamantyl-1H-1,2,3-triazole (*m*-L2): Prepared using the same procedure as that for *o*-L2, replacing benzyl

azide with adamantyl azide (72% yield). ^1H NMR (300 MHz, CDCl_3 , δ , ppm): 8.07 (d, $^3J = 6.2\text{ Hz}$, 2H), 7.94 (s, 1H), 7.79 (s, 1H), 7.50–7.40 (m, 2H), 6.85 (s, 4H), 2.40–2.20 (m, 15H), 2.04 (s, 12H), 1.83 (s, 6H). ^{13}C NMR (100 MHz, CDCl_3 , δ , ppm): 145.2, 139.4, 137.2, 131.2, 127.8, 127.0, 126.7, 114.8, 103.1, 58.1, 41.5, 34.4, 28.0, 22.0, 19.7.

8.3. Syntheses of Pt(II) Compounds

The general procedures for each class of Pt(II) compounds are provided below. The yields for all Pt(II) compounds are based on the recrystallized products. ^{13}C NMR spectra were not recorded for all Pt(II) compounds because of their poor solubility. The Pt(II) compounds have the tendency to co-crystallize with solvent molecules such as THF and CH_2Cl_2 . For some of the compounds, the solvent molecules were positively identified in the crystal lattice of the Pt(II) compounds. For elemental analysis, all samples were dried under vacuum at ambient temperature. Nonetheless, many of the compounds still show solvent molecules trapped inside the crystal lattice.

General Procedure for the Synthesis of Pt(II) Compounds 1–3. The Bptrz ligand (0.10 mmol) and $[\text{PtMe}_2(\text{SMe}_2)]_2$ (0.055 mmol) were added to a 20 mL screw-cap vial with 5 mL of acetone. The mixture was heated at 70 °C for 3 hours before 1 mL of 0.1 M solution of TsOH in THF was added. The resulting solution was stirred for 1 hour, then 2 mL of 0.1 M solution of Na(β -diketonate) in methanol was added and the mixture was stirred overnight. After the solvent was removed under reduced pressure, the product was extracted with dichloromethane, and then washed with brine and water. The combined organic phase was dried over MgSO_4 , filtered and purified using a column chromatography on silica using dichloromethane as eluent. The compound was further purified by recrystallization from either CH_2Cl_2 or THF.

(*p*-L1)Pt(acac) (**1**): (24% yield). ^1H NMR (400 MHz, CD_2Cl_2 , δ , ppm): 7.51 (s, 1H), 7.47 (s, 1H), 7.40–7.28 (m, 5H), 7.11 (d, $^3J = 7.6\text{ Hz}$, 1H), 7.07 (d, $^3J = 7.6\text{ Hz}$, 1H), 6.74 (s, 4H), 5.49 (s, 2H), 5.37 (s, 1H), 2.20 (s, 6H), 1.97 (s, 12H), 1.88 (s, 3H), 1.60 (s, 3H). Anal. calcd for $\text{C}_{38}\text{H}_{40}\text{BN}_3\text{O}_2\text{Pt}$: C 58.77, H 5.19, N 5.41; found: C 58.76, H 5.21, N 5.39.

Characterization data for (*m*-L1)Pt(acac) (**2**) and (*m*-L2)Pt(acac) (**3**) can be found in the supporting materials.

General Procedure for the Synthesis of Pt(II) Compounds 4–7. The Bptrz ligand (0.10 mmol) and $[\text{PtMe}_2(\text{SMe}_2)]_2$ (0.055 mmol) were added to a 20 mL screw-cap vial with 5 mL of acetone. The mixture was heated at 70 °C for 3 hours before 1 mL of 0.1 M solution of the corresponding picolinic acid in methanol was added. The resulting solution was stirred overnight. The product was filtered and washed with hexane, diethyl ether and methanol, sequentially. The product was purified and isolated by recrystallization from either THF or CH_2Cl_2 or a mixture of them with the addition of hexane or methanol.

(*p*-L1)Pt(pic) (**4**): (26% yield). ^1H NMR (500 MHz, CD_2Cl_2 , δ , ppm): 9.52 (d, $^3J = 5.6\text{ Hz}$, 1H), 8.14 (m, 1H), 7.80 (s, 1H), 7.70 (m, 1H), 7.62 (s, 1H), 7.50–7.42 (m, 5H), 7.27 (d, $^3J = 7.5\text{ Hz}$, 1H), 7.16 (d, $^3J = 7.5\text{ Hz}$, 1H), 6.88 (s, 4H), 5.64 (s, 2H), 2.34 (s, 6H), 2.06 (s, 12H). Anal. calcd for 4-THF ($\text{C}_{43}\text{H}_{45}\text{BN}_4\text{O}_3\text{Pt}$): C 59.24, H 5.20, N 6.42; found: C 59.83, H 5.18, N 6.44.

Characterization data for (*m*-L1)Pt(pic) (**5**), (*m*-L1)Pt(4-Me-pic) (**6**), (*m*-L2)Pt(4-Me-pic) (**7**), and (*m*-L2)Pt(pic) (**7a**) are provided in the supporting materials.

General Procedure for the Synthesis of Pt(II) Compounds 8–11. The ancillary ligand *t*-Bu-pytrz-Me and CF_3 -pytrz-Me were synthesized according to literature procedure.^[4]

The Bptrz ligand (0.10 mmol) and $[\text{PtMe}_2(\text{SMe}_2)]_2$ (0.055 mmol) were added to a 20 mL screw-cap vial with 5 mL of acetone. The mixture was heated at 70 °C for 3 hours before 1 mL of 0.1 M solution of TsOH in acetone was added. The resulting solution was stirred for 1 hour, then 0.13 mmol of corresponding pytrz ligand in acetone was added and the mixture was stirred at RT for 3 days. The product was filtered and washed with hexane, diethyl ether and methanol, sequentially. The product was further purified via chromatography and recrystallization

from CH_2Cl_2 or THF with hexane. Unless specified, compounds **8–11** refer to the N^1 -*trans* isomers.

(*m*-L1)Pt(pytrz) (**8**): (23% yield). ^1H NMR (400 MHz, CD_2Cl_2 , δ , ppm): 9.76 (d, $^3J = 6\text{ Hz}$, 1H), 9.12 (d, $^3J = 7.6\text{ Hz}$, 1H), 8.16–8.09 (m, 3H), 7.65 (s, 1H), 7.50–7.40 (m, 7H), 7.33 (dd, $^3J = 7.8\text{ Hz}$, $^4J = 1.5\text{ Hz}$, 1H), 6.85 (s, 4H), 5.65 (s, 2H), 2.33 (s, 6H), 2.05 (s, 12H). Anal. calcd for **8**·0.5 CH_2Cl_2 ($\text{C}_{40.5}\text{H}_{39}\text{BCIN}_7\text{Pt}$): C 56.23, H 4.54, N 11.33; found: C 56.38, H 4.84, N 10.90.

(*m*-L1)Pt(*t*-Bu-pytrz-Me) (**9**), (*m*-L1)Pt(CF_3 -pytrz-Me) (**10**) and (*m*-L2)Pt(CF_3 -pytrz-Me) (**11**) are provided in the supporting materials.

8.4. EL Device Fabrication

Devices were fabricated in a three-chamber evaporator (EL-OEL cluster tool) with a base pressure of $\sim 1 \times 10^{-5}$ Pa without breaking vacuum. The ITO anode is commercially patterned and coated on glass substrates $50 \times 50\text{ mm}^2$ with a sheet resistance less than 15 Ω . Substrates were ultrasonically cleaned with a standard regiment of Alconox, acetone, and methanol followed by UV ozone treatment for 15 min. The active area for all devices was 2 mm^2 . The film thicknesses were monitored by a calibrated quartz crystal microbalance and were further verified for single-carrier devices using capacitance-voltage measurements (Agilent 4294A). I-V characteristics were measured using a HP4140B picoammeter in ambient air. Luminance measurements and EL spectra were taken using a Minolta LS-110 luminance meter and an Ocean Optics USB200 spectrometer with bare fiber, respectively. The external quantum efficiency of EL devices was calculated following the standard procedure.^[38] After deposition, single carrier devices were transferred to a homebuilt variable temperature cryostat for measurement at 298 K. UPS measurements were performed using a PHI 5500 MultiTechnique system, with attached organic deposition chamber with a base pressure of 10^{-10} Torr. Additional details regarding device fabrication, characterization and UPS measurements have been described elsewhere.^[39,40]

8.5. X-ray Crystallography Analysis

Single crystals of **1**, **4–6**, **7a**, and **8–10** were obtained from either CH_2Cl_2 or THF by slow evaporation of the solvent. For some of the compounds, it was necessary to add either methanol or hexanes to facilitate the crystal growth. The crystals were mounted on glass fibers and the data were collected on a Bruker Apex II single-crystal X-ray diffractometer with graphite-monochromated $\text{Mo K}\alpha$ radiation, operating at 50 kV and 30 mA, and at 180 K. Data were processed on a PC with the aid of the Bruker SHELXTL software package (version 6.14)^[41] and corrected for absorption effects. All structures were solved using direct methods. CH_2Cl_2 solvent molecules were located in the lattices of **9** and **10** and refined successfully. THF and methanol were located in the crystal lattice of **5** and were modelled and refined successfully. THF solvent molecules were located in the crystal lattices of **6** and **7a**, which were all modelled and refined successfully except one disordered THF molecule in **7a** that was removed by the Platon^[42] Squeeze routine to improve the quality of the structural data. All non-hydrogen atoms were refined anisotropically. Complete crystal structural data can be found in the supporting information. [CCDC 955635–955642 contains the supplementary crystallographic data for this paper. These data can be obtained free of charge from The Cambridge Crystallographic Data Centre via www.ccdc.cam.ac.uk/data_request/cif.]

Supporting Information

Supporting Information is available from the Wiley Online Library or from the author.

Acknowledgements

We thank the Natural Sciences and Engineering Research Council of Canada for financial support. S. Wang thanks the Canada Council for the Arts for the Killam Research Fellowship.

Received: August 15, 2013

Revised: October 3, 2013

Published online: December 4, 2013

- [1] a) H. Fu, Y.-M. Cheng, P.-T. Chou, Y. Chi, *Mater. Today* **2011**, 14, 472; b) Y. Chi, P. T. Chou, *Chem. Soc. Rev.* **2010**, 39, 638; c) Y. You, S. Y. Park, *Dalton Trans.* **2009**, 1267; d) C.-L. Ho, W.-Y. Wong, *New J. Chem.* **2013**, 37, 1665.
- [2] a) A. B. Tamayo, B. D. Alleyne, P. I. Djurovich, S. Lamansky, I. Tsyba, N. N. Ho, R. Bau, M. E. Thompson, *J. Am. Chem. Soc.* **2003**, 125, 7377; b) J. Li, P. I. Djurovich, B. D. Alleyne, M. Yousufuddin, N. N. Ho, J. C. Thomas, J. C. Peters, R. Bau, M. E. Thompson, *Inorg. Chem.* **2005**, 44, 1713; c) R. J. Holmes, B. W. D'Andrade, S. R. Forrest, X. Ren, M. E. Thompson, *Appl. Phys. Lett.* **2003**, 83, 3818.
- [3] S.-C. Lo, C. P. Shipley, R. N. Bera, R. E. Harding, A. R. Cowley, P. L. Burn, I. D. W. Samuel, *Chem. Mater.* **2006**, 18, 5119.
- [4] E. Orselli, G. S. Kottas, A. E. Konradsson, P. Coppo, R. Fröhlich, L. D. Cola, A. V. Dijken, M. Büchel, H. Börner, *Inorg. Chem.* **2007**, 46, 11082.
- [5] C.-J. Chang, C.-H. Yang, K. Chen, Y. Chi, C.-F. Shu, M.-L. Ho, Y.-S. Yeh, P.-T. Chou, *Dalton Trans.* **2007**, 1881.
- [6] Y.-S. Yeh, Y.-M. Cheng, P.-T. Chou, G.-H. Lee, C.-H. Yang, Y. Chi, C.-F. Shu, C.-H. Wang, *ChemPhysChem* **2006**, 7, 2294.
- [7] C.-F. Chang, Y.-M. Cheng, Y. Chi, Y.-C. Chiu, C.-C. Lin, G.-H. Lee, P.-T. Chou, C.-C. Chen, C.-H. Chang, C.-C. Wu, *Angew. Chem., Int. Ed.* **2008**, 47, 4542.
- [8] V. Sivasubramaniam, F. Brodtkorb, S. Hanning, H. P. Loebl, V. V. Elsbergen, H. Boerner, U. Scherf, M. Kreyenschmidt, *J. Fluor. Chem.* **2009**, 130, 640.
- [9] a) R. Seifert, I. R. D. Moraes, S. Scholz, M. C. Gather, B. Lüssem, K. Leo, *Org. Electronics* **2013**, 14, 115; b) E. Baranoff, S. Suárez, P. Bugnon, C. Barolo, R. Buscaino, R. Scopelliti, L. Zuppiroli, M. Graetzel, Md. K. Nazeeruddin, *Inorg. Chem.* **2008**, 47, 6675.
- [10] a) Y.-C. Chiu, Y. Chi, J.-Y. Hung, Y.-M. Cheng, Y.-C. Yu, M.-W. Chung, G.-H. Lee, P.-T. Chou, C.-C. Chen, C.-C. Wu, H.-Y. Hsieh, *ACS Appl. Mater. Interfaces* **2009**, 1, 433; b) C.-H. Lin, Y.-Y. Chang, J.-Y. Hung, C.-Y. Lin, Y. Chi, M.-W. Chung, C.-L. Lin, P.-T. Chou, G.-H. Lee, C.-H. Chang, W.-C. Lin, *Angew. Chem. Int. Ed.* **2011**, 50, 3182; c) C.-H. Chang, C.-L. Ho, Y.-S. Chang, I.-C. Lien, C.-H. Lin, Y.-W. Yang, J.-L. Liao, Y. Chi, *J. Mater. Chem. C* **2013**, 1, 2639.
- [11] a) J. Kavitha, S.-Y. Chang, Y. Chi, J.-K. Yu, Y.-H. Hu, P.-T. Chou, S.-M. Peng, G.-H. Lee, Y.-T. Tao, C.-H. Chien, A.-J. Carty, *Adv. Funct. Mater.* **2005**, 15, 223; b) S.-Y. Chang, J. Kavitha, J.-Y. Hung, Y. Chi, Y.-M. Cheng, E. Y. Li, P.-T. Chou, G.-H. Lee, A. J. Carty, *Inorg. Chem.* **2007**, 46, 7064; c) S.-Y. Chang, Y.-M. Cheng, Y. Chi, Y.-C. Lin, C.-M. Jiang, G.-H. Lee, P.-T. Chou, *Dalton Trans.* **2008**, 6901.
- [12] a) W.-Y. Wong, Z. He, S.-K. So, K.-L. Tong, Z. Lin, *Organometallics* **2005**, 24, 4079; b) G. Zhou, Q. Wang, X. Wang, C.-L. Ho, W.-Y. Wong, D. Ma, L. Wang, Z. Lin, *J. Mater. Chem.* **2010**, 20, 7472; c) G. J. Zhou, C. L. Ho, W. Y. Wong, Q. Wang, D. G. Ma, L. X. Wang, Z. Y. Lin, T. B. Marder, A. Beebe, *Adv. Funct. Mater.* **2008**, 18, 499; d) M. Cocchi, D. Virgili, V. Fattori, D. L. Rochester, J. A. G. Williams, *Adv. Funct. Mater.* **2007**, 17, 285.
- [13] a) Z. M. Hudson, C. Sun, M. G. Helander, H. Amarné, Z.-H. Lu, S. Wang, *Adv. Funct. Mater.* **2010**, 20, 3426; b) Z. M. Hudson, S. Wang, *Dalton Trans.* **2011**, 40, 7805; c) Z. Wang, M. G. Helander, Z. M. Hudson, J. Qiu, S. Wang, Z.-H. Lu, *Appl. Phys. Lett.* **2011**, 98, 213301; d) Z. M. Hudson, M. G. Helander, Z.-H. Lu, S. Wang, *Chem. Commun.* **2011**, 47, 755.
- [14] X.-C. Hang, T. Fleetham, E. Turner, J. Brooks, J. Li, *Angew. Chem. Int. Ed.* **2013**, 52, 6753.
- [15] X. Yang, Z. Wang, S. Madakuni, J. Li, G. E. Jabbour, *Adv. Mater.* **2008**, 20, 2405.
- [16] a) M. Cocchi, J. Kalinowski, V. Fattori, J. A. G. Williams, L. Murphy, *Appl. Phys. Lett.* **2009**, 94, 073309; c) J. A. G. Williams, S. Develay, D. L. Rochester, L. Murphy, *Coord. Chem. Rev.* **2008**, 252, 2596; d) L. Murphy, P. Brulatti, V. Fattori, M. Cocchi, J. A. G. Williams, *Chem. Commun.* **2012**, 48, 5817.
- [17] X. Zhang, A. M. Wright, N. J. DeYonker, T. K. Hollis, N. I. Hammer, C. E. Webster, E. J. Valente, *Organometallics* **2012**, 31, 1664.
- [18] Y. Rao, D. Schoenmakers, Y.-L. Chang, J. Lu, Z.-H. Lu, Y. Kang, S. Wang, *Chem. Eur. J.* **2012**, 18, 11306.
- [19] Z. M. Hudson, C. Sun, M. G. Helander, Y.-L. Chang, Z.-H. Lu, S. Wang, *J. Am. Chem. Soc.* **2012**, 134, 13930.
- [20] J. Brooks, Y. Babayan, S. Lamansky, P. I. Djurovich, I. Tsyba, R. Bau, M. E. Thompson, *Inorg. Chem.* **2002**, 41, 3055.
- [21] B. Beyer, C. Ulbricht, D. Escudero, C. Friebe, A. Winter, L. González, U. S. Schubert, *Organometallics* **2009**, 28, 5478.
- [22] H. C. Kolb, M. G. Finn, K. B. Sharpless, *Angew. Chem. Int. Ed.* **2001**, 40, 2004.
- [23] V. V. Rostovtsev, L. G. Green, V. V. Fokin, K. B. Sharpless, *Angew. Chem. Int. Ed.* **2002**, 41, 2596.
- [24] Z. M. Hudson, B. A. Blight, S. Wang, *Org. Lett.* **2012**, 14, 1700.
- [25] S.-B. Ko, J.-S. Lu, Y. Kang, S. Wang, *Organometallics* **2013**, 32, 599.
- [26] C. D. Pietro, S. Serroni, S. Campagna, T. Gandolfi, R. Ballardini, S. Fanni, W. R. Browne, J. G. Vos, *Inorg. Chem.* **2002**, 41, 2871.
- [27] a) J. A. G. Williams, *Top. Curr. Chem.* **2007**, 281, 205; b) P. Du, J. Schneider, W. W. Brennessel, R. Eisenberg, *Inorg. Chem.* **2008**, 47, 69; c) T. J. Wadas, Q.-M. Wang, Y. Kim, C. Flaschenreim, T. N. Blanton, R. Eisenberg, *J. Am. Chem. Soc.* **2004**, 126, 16841; d) V. W.-W. Yam, E. C.-C. Cheng, *Chem. Soc. Rev.* **2008**, 37, 1806; e) Z. He, W.-Y. Wong, X. M. Yu, H.-S. Kwok, Z. Y. Lin, *Inorg. Chem.* **2006**, 45, 10922.
- [28] S. J. Farley, D. L. Rochester, A. L. Thompson, J. A. K. Howard, J. A. G. Williams, *Inorg. Chem.* **2005**, 44, 9690.
- [29] Á. Díez, J. Forníes, C. Larraz, E. Laliñe, J. A. López, A. Martín, M. T. Moreno, V. Sicilia, *Inorg. Chem.* **2010**, 49, 3239.
- [30] H. Sasabe, J. Kido, *J. Mater. Chem. C* **2013**, 1, 1699.
- [31] a) Y. Sun, N. C. Giebink, H. Kanno, B. Ma, M. E. Thompson, S. R. Forrest, *Nature* **2006**, 440, 908; b) B. W. D'Andrade, S. R. Forrest, *Adv. Mater.* **2004**, 16, 1585; c) E. L. Williams, K. Haavisto, J. Li, G. E. Jabbour, *Adv. Mater.* **2007**, 19, 197; d) M. Cocchi, J. Kalinowski, D. Virgili, V. Fattori, S. Develay, J. A. G. Williams, *Appl. Phys. Lett.* **2007**, 90, 163508; e) G. J. Zhou, W.-Y. Wong, S. Suo, J. Photochem, *Photobio. C: Photochem. Rev.* **2010**, 11, 133.
- [32] M. J. Frisch, G. W. Trucks, H. B. Schlegel, G. E. Scuseria, M. A. Robb, J. R. Cheeseman, J. A. Montgomery, Jr., T. Vreven, K. N. Kudin, J. C. Burant, J. M. Millam, S. S. Iyengar, J. Tomasi, V. Barone, B. Mennucci, M. Cossi, G. Scalmani, N. Rega, G. A. Petersson, H. Nakatsuji, M. Hada, M. Ehara, K. Toyota, R. Fukuda, J. Hasegawa, M. Ishida, T. Nakajima, Y. Honda, O. Kitao, H. Nakai, M. Klene, X. Li, J. E. Knox, H. P. Hratchian, J. B. Cross, C. Adamo, J. Jaramillo, R. Gomperts, R. E. Stratmann, O. Yazyev, A. J. Austin, R. Cammi, C. Pomelli, J. W. Ochterski, P. Y. Ayala, K. Morokuma, G. A. Voth, P. Salvador, J. J. Dannenberg, V. G. Zakrzewski, S. Dapprich, A. D. Daniels, M. C. Strain, O. Farkas, D. K. Malick, A. D. Rabuck,

- K. Raghavachari, J. B. Foresman, J. V. Ortiz, Q. Cui, A. G. Baboul, S. Clifford, J. Cioslowski, B. B. Stefanov, G. Liu, A. Liashenko, P. Piskorz, I. Komaromi, R. L. Martin, D. J. Fox, T. Keith, M. A. Al-Laham, C. Y. Peng, A. Nanayakkara, M. Challacombe, P. M. W. Gill, B. Johnson, W. Chen, M. W. Wong, C. Gonzalez, J. A. Pople, Gaussian 03, revision C.02; Gaussian, Inc.: Wallingford, CT, **2004**.
- [33] a) L. Xiao, Z. Chen, B. Qu, J. Luo, S. Kong, Q. Gong, J. Kido, *Adv. Mater.* **2011**, *23*, 926; b) K. S. Yook, J. Y. Lee, *Adv. Mater.* **2012**, *24*, 3169.
- [34] a) H. Z. Siboni, H. Aziz, *Org. Electronics* **2013**, *14*, 2510; b) G.-J. Zhou, W.-Y. Wong, B. Yao, Z. Y. Xie, L. X. Wang, *J. Mater. Chem.* **2008**, *18*, 1799.
- [35] a) T. Fleetham, J. Ecton, Z. X. Wang, N. Bakken, J. Li, *Adv. Mater.* **2013**, *25*, 2573; b) G. J. Zhou, Q. Wang, C.-L. Ho, W.-Y. Wong, D. G. Ma, L. X. Wang, *Chem. Commun.* **2009**, 3574.
- [36] Z. An, S. A. Odom, R. F. Kelley, C. Huang, X. Zhang, S. Barlow, L. A. Padilha, J. Fu, S. Webster, D. J. Hagan, E. W. Van Stryland, M. R. Wasielewski, S. R. Marder, *J. Phys. Chem. A* **2009**, *113*, 5585.
- [37] A. Fukazawa, H. Yamada, S. Yamaguchi, *Angew. Chem. Int. Ed.* **2008**, *47*, 5582.
- [38] S. R. Forrest, D. D. C. Bradley, M. E. Thompson, *Adv. Mater.* **2003**, *15*, 1043.
- [39] M. G. Helander, Z. B. Wang, M. T. Greiner, J. Qiu, Z. H. Lu, *Rev. Sci. Instrum.* **2009**, *80*, 033901.
- [40] M. G. Helander, M. T. Greiner, Z. B. Wang, Z. H. Lu, *Appl. Surf. Sci.* **2010**, *256*, 2602.
- [41] Shelxtl Version 6.14, Bruker Analytical X-ray Systems, copyright 2000-2003.
- [42] a) A. L. Spek, *Acta Cryst.* **2009**, *D65*, 148; b) *PLATON-A Multipurpose Crystallographic Tool* (Ed: A. P. Spek), Utrecht University, Utrecht, The Netherlands **2011**.